Constitutive Modeling for Two Sands under High Pressure

Yang Xiao, M. ASCE; Chenggui Wang; Zhichao Zhang; Hanlong Liu; and Zhen-yu Yin

Abstract: Particle breakage is a typical characteristic of crushable granular soil under high pressure, which has great effects on its stress-strain behaviors. The phenomenon of critical state line (CSL) shifting downwards in the compression plane caused by particle breakage was depicted by a breakage-dependent critical state plane (BCSP). Particle breakage was incorporated into a void-ratio-pressure state parameter to modify Rowe's stress-dilatancy equation, and then the state parameter was incorporated into the bounding stress ratio and plastic modulus. Due to the impact of high pressure on particle breakage, the pressure-dependent plastic modulus parameters were introduced. A breakage-dependent bounding surface plasticity model was proposed to capture the influence of particle breakage on the state-dependent stress-strain behaviors for silica and coral sands and the transition of complex breakage-dependent critical states resulted from the competition between the contraction due to particle breakage and the dilatancy due to particle rearrangement.

Keywords: plasticity; constitutive model; particle breakage; critical state; state parameter; dilatancy

----

Yang Xiao, M. ASCE

Professor, Key Laboratory of New Technology for Construction of Cities in Mountain Area, State Key Laboratory of Coal Mine Disaster Dynamics and Control, School of Civil Engineering, Chongqing University, Chongqing, 400045, China. Email: hhuxyanson@163.com

Chenggui Wang

Ph.D. Candidate, School of Civil Engineering, Chongqing University, Chongqing, 400045, China. Email: cgwangic@163.com

Zhichao Zhang

Associate Professor, School of Civil Engineering, Chongqing University, Chongqing, 400045, China. Email: zczhang15@cqu.edu.cn (Corresponding Author)

Hanlong Liu

Professor and Vice President, Chongqing University, Chongqing, 400450, China. Email: cehliu@cqu.edu.cn

Zhen-yu Yin

Associate Professor, Department of Civil and Environmental Engineering, The Hong Kong Polytechnic University, Hung Hom, Kowloon, Hong Kong, China. E-mail: zhenyu.yin@gmail.com

Introduction

Crushable granular materials are easily prone to fracturing when they are subjected to high pressure (Hagerty et al. 1993; Lade et al. 1996; Yamamuro et al. 1996; Nakata et al. 2001; Hyodo et al. 2016; Zheng and Tannant 2016; Man and Chik-Kwong Wong 2017; Mun and McCartney 2017; Yu 2017b; Mao et al. 2018; Yu 2019; Mao et al. 2020; Wu et al. 2020), large displacement (Luzzani and Coop 2002; Coop et al. 2004; Wafid Agung et al. 2004; Fukuoka et al. 2006; Hiroshi et al. 2006; Sadrekarimi and Olson 2010, 2011b; Miao and Airey 2013; Zhang and Baudet 2013; Wei et al. 2018), high strain rate (Omidvar et al. 2012; Huang et al. 2014; Suescun-Florez et al. 2015; Huang et al. 2017; Parab et al. 2017; Xiao et al. 2019b), high frequency (Sun et al. 2015; Indraratna et al. 2020), complex loading conditions (Liu et al. 2020; Ning et al. 2020; Pan et al. 2020), and a series of drying-wetting cycles or flooding (Ovalle et al. 2015; Alonso et al. 2016; Mun and McCartney 2017; Chen et al. 2020; Tong et al. 2020), especially in the pile installation, and high rockfill dam, etc. Particle breakage has great influences on the deformation and strength of sands, which leads to an increase in volume strain and a decrease in peak strength (Hagerty et al. 1993; Nakata et al. 1999; Luzzani and Coop 2002; Coop et al. 2004; Russell and Khalili 2004; Tarantino and Hyde 2005; Lobo-Guerrero and Vallejo 2006; Valdes and Koprulu 2007; Kuwajima et al. 2009; Lade et al. 2009; Bandini and Coop 2011; Wang et al. 2011; Zhang and Baudet 2013; Yu 2017b, 2019). The extent of particle breakage would be determined by the coordinate numbers and internal flows of particles (McDowell et al. 1996; McDowell and Bolton 1998; Ueng and Chen 2000; Liu et al. 2019). In addition, particle breakage intensifies with increases in particle size and angularity and decreases in mineral strength, uniformity coefficient, density and biobonding (Hardin 1985; Yamamuro et al. 1996; Nakata et al. 1999; McDowell and Amon 2000; Hyodo et al. 2016; Xiao et al. 2019a; Xiao et al. 2020).

It is great challenging to precisely predict the deformation and strength of granular soils under high pressure using a set of unique model parameters. Ueng and Chen (2000) studied the effect of particle breakage on the shear strength of sands by considering the energy consumption correlated to the rate of increment in particle surface area per unit volume of sand, which has also been extended to other crushable soils (Indraratna and Salim 2002; Salim and Indraratna 2004; Tarantino and Hyde 2005). Varadarajan et al. (2006) applied the framework of disturbed state concept (Desai 2000) to establish an elastoplastic model by introducing a degradation function (Varadarajan et al. 2003) to consider the effect of particle breakage on the stress-strain relationship of rockfill materials. Russell and Khalili (2004) proposed a model within the critical state framework based on a critical state line (CSL) consisting of three linear segments (a complex function) to account for the influence of particle breakage. In addition, the breakage theory proposed by Einav (2007) was effectively used to establish a breakage-dependent elastoplastic constitutive model in the thermodynamic framework to capture the effects of particle breakage evolution on the stress-strain relation (Tengattini et al. 2016; Zhang et al. 2016; Chang et al. 2019; Cil et al. 2020). A notion of dynamic CSL due to particle breakage (Daouadji et al. 2001; Muir Wood and Maeda 2008) has been widely accepted to establish breakage-dependent models, e.g., elastoplastic models with different yielding mechanisms (Daouadji and Hicher 2010; Hu et al. 2011; Yin et al. 2017), elastoplastic models in the framework of bounding surface plasticity (Kan and Taiebat 2014; Indraratna et al. 2015; Chen et al. 2016; Xiao and Liu 2017), elastoplastic models in the framework of generalized plasticity (Liu and Zou 2013; Liu and Gao 2017).

State-dependent behaviors of granular soils (Bolton 1986; Been et al. 1991; Yu 1998; Salgado et al. 2000; Chu and Leong 2002; Xiao et al. 2014; Lashkari 2016) are significant when analyzing the deformation and stability of slopes, embankments, dams, coastal engineering, etc. The state indices referring to CSL are effective parameters to unify strength and dilatancy (Been and Jefferies 1985; Yang and Li 2004; Chiu and Fu 2008; Chu and Wanatowski 2008, 2009; Rabbi et al. 2019) and also to establish a unified state-dependent constitutive model (Jefferies 1993; Muir Wood et al. 1994; Gajo and Muir Wood 1999; Li and Dafalias 2000; Yao et al. 2004; Ling and Yang 2006; Lashkari and Yaghtin 2018; Sun et al. 2019; Wei and Yang 2019; Yang et al. 2019; Sun et al. 2020). The dilatancy equation proposed by Rowe (1962) is widely applied in constitutive models to simulate the state-dependent dilatancy behavior by incorporating a state parameter (Wan and Guo 1998; Xu and Song 2009; Xiao et al. 2017). Xiao and Liu (2017) proposed a void-ratio-pressure state parameter by combining a void-ratio state parameter (Wan and Guo 1998) and a pressure state parameter (Wang et al. 2002), which is appropriate for crushable soils with a wide range of confining pressures and void ratios. However, the state parameter and state-dependent dilatancy considering the evolution of particle breakage for sands under high pressure have not been fully understood and thereby need to be further investigated.

The main objective of this paper is to establish a breakage-dependent plasticity model for sands using the revised Rowe's stress-dilatancy equation by incorporating a void-ratio-pressure state parameter in the framework of the extended breakage-dependent critical state theory.

Constitutive Model

The bounding surface plasticity model (Dafalias and Popov 1976) can capture the volumetric expansion and strain softening of granular soils (Bardet 1986; Li and Dafalias 2000; Russell and Khalili 2004; Kan Mojtaba et al. 2014). The framework proposed by Li and Dafalias (2000) was adopted to establish the constitutive equations. However, it is noted that the mechanical behaviors of granular materials are always affected by particle breakage (Ueng and Chen 2000; Coop et al. 2004; Russell and Khalili 2004; Zhang and Baudet 2013; Hyodo et al. 2016; Yu 2017b; Mao et al. 2019; Ovalle and Hicher 2019; Ganju et al. 2020), which reduces the dilatancy and peak strength, and enhances the hardening and contraction behaviors of sands (Indraratna and Salim 2002; Hasanlourad et al. 2008; Sadrekarimi and Olson 2011a; Zhang et al. 2013; Liu et al. 2016; Yu 2017b; Ciantia and O'Sullivan 2020; Wang et al. 2020; Zhang and Luo 2020). Thereby, the influences of particle breakage on the critical state and the state-dependent behaviors of sands must be considered. The breakage-dependent critical state plane (BCSP) and the corresponding state parameter will be defined in the following Sections.

Breakage-Dependent Critical State Plane

Particle breakage leads to the upward-shifting of grading curves and the dynamic change of material structure as the large-size particles break into small-size particles, which fill the void among the remnant larger ones (Hardin 1985; McDowell and Bolton 1998; Daouadji et al. 2001). Lade et al. (1996) used a hyperbolic model to establish the relationship between relative breakage and total input energy per unit volume. Yu (2017a) and Jia et al. (2017) employed the plastic work per unit volume W_p instead of the total input energy (Lade et al. 1996), and found the relationship between B_r and W_p can also be expressed as a hyperbolic function:

$$B_r = \frac{W_p}{\chi_W + k_W W_p} \quad \textbf{(1)}$$

where B_r is the particle breakage index defined by Hardin (1985); χ_W and k_W are material parameters. χ_W = 7.847 MJ/m^3 and k_W = 1.686 for silica sands NO.5 (Yu 2017a) while χ_W = 4.820 MJ/m^3 and k_W = 3.228 for coral sands NO.3 (Yu 2018). The plastic work W_p can be calculated by:

$$W_p = \int dW_p = \int \left(p' d\varepsilon_v^p + q d\varepsilon_s^p \right) \quad \textbf{(2)}$$

where $d\varepsilon_v^p$ is the plastic volumetric strain increment; $d\varepsilon_s^p$ is the plastic shear strain increment; p' is the mean effective stress; and q is the deviatoric stress.

Based on the phenomenon that the CSL shifts downwards in the compression plane (i.e., void ratio e versus logarithm of mean effective stress $\ln p'$) due to particle breakage (Muir Wood and Maeda 2008; Kikumoto et al. 2010; Bandini and Coop 2011; Ghafghazi et al. 2014; Indraratna et al. 2015; Heitor et al. 2016; Altuhafi et al. 2018; Ciantia et al. 2019), the data of silica sands NO.5 (Yu 2017a) in **Figs. 1(a)-1(b)** and coral sands NO.3 (Yu 2018) in **Figs. 1(c)-1(d)** are presented to illustrate the dynamic transition of breakage-dependent critical state line (BCSL) due to grain crushing. According to previous work (Yu 2019), the slope of BCSL in the compression plane with a neglectable grain crushing was approximated as 0.1. **Figs. 1(a)-1(b)** show the transition of BCSL of silica sand with the same void ratio of 0.798 under different confining pressures while **Figs. 1(c)-1(d)** present the transition of BCSL of coral sand with different initial void ratios under the same confining pressure of 3 MPa. The red line in **Fig. 1** is the BCSL with B_r = 0, and the blue lines are a series of BCSLs with different B_r values for the corresponding critical state points (CSPs). The evolution of BCSL is shown in **Figs. 1(b)** and **1(d)** with a normal coordinate and in **Figs. 1(a)** and **1(c)** with a semi-logarithmic coordinate.

Following the concept of BCSP in the B_r - e - p' space proposed by Xiao and Liu (2017), the BCSP for silica sand in **Figs. 2(a)-2(b)** and coral sand in **Fig. 2(c)** can be defined as:

$$e_{cs} = e_{cs0} - \lambda \ln p'_{cs} \quad \textbf{(3)}$$

$$e_{cs} = e_{cs0} - \lambda \ln p'_{cs} = e_{cs0}\left(B_r\right) - \lambda \ln p'_{cs} \quad \textbf{(4)}$$

where e_{cs} is the critical-state void ratio; p'_{cs} is the critical-state mean effective stress; e_{cs0} is the initial critical-state void ratio; λ is the slope of the BCSL. According to the finding by Xiao and Liu (2017), the relationship between e_{cs0} and B_r can be expressed as an exponential function:

$$e_{cs0} = e_{B0} - k_B \exp\left(\chi_B B_r\right) \tag{5}$$

where e_{B0}, k_B and χ_B are the breakage-dependent critical-state parameters. Substituting **Eq. (5)** into **Eq. (4)**, the BCSP can be given as:

$$e_{cs} = e_{B0} - k_B \exp\left(\chi_B B_r\right) - \lambda \ln p'_{cs} \tag{6}$$

Equation (6) suggests that an increase in B_r leads to a downward movement of the BCSL, which is in agreement with the test observations (Kikumoto et al. 2010; Bandini and Coop 2011; Ghafghazi et al. 2014; Indraratna et al. 2015; Heitor et al. 2016; Altuhafi et al. 2018). Combination of **Eqs. (1)** and **(6)** gives:

$$e_{cs} = e_{B0} - \lambda \ln p'_{cs} - k_B \exp\left(\chi_B \frac{W_p}{\chi_W + k_W W_p}\right) \tag{7}$$

Equation (7) indicates that the location of CSL during grains crushing is determined by the plastic work W_p, as shown in **Figs. 3(a)-3(b)** for silica sand and **Fig. 3(c)** for coral sand, which is in line with the findings by Liu and Zou (2013).

State Parameter

A void-ratio-pressure state parameter suggested by Xiao and Liu (2017) that combines the void-ratio state parameter defined by Wan and Guo (1998) and the pressure state parameter proposed by Wang et al. (2002), as shown in **Fig. 1**, is adopted in this study:

$$I_{ep} = \frac{e}{e_{cs}} \frac{p'}{p'_{cs}} \tag{8}$$

As shown in **Fig. 1**, **Eq. (6)** can be further rewritten by substituting p'_{cs} with p':

$$e_{cs} = e_{B0} - k_B \exp\left(\chi_B B_r\right) - \lambda \ln p' \tag{9}$$

Similarly, substituting e_{cs} with e into **Eq. (6)** gives:

$$p'_{cs} = \exp\left\{(1/\lambda)\left[e_{B0} - k_B \exp\left(\chi_B B_r\right) - e\right]\right\} \quad \textbf{(10)}$$

Substituting **Eqs. (9)** and **(10)** into **Eq. (8)** yields

$$I_{ep} = \frac{\dfrac{ep'}{e_{B0} - k_B \exp\left(\chi_B B_r\right) - \lambda \ln p'}}{\exp\left[\dfrac{e_{B0} - k_B \exp\left(\chi_B B_r\right) - e}{\lambda}\right]} \quad \textbf{(11)}$$

The values of void-ratio-pressure state parameter I_{ep} from the initial state point (ISP) to the critical state point (CSP) during the shearing process are calculated and labelled in **Figs. 2-3**. A specimen is defined as loose if the initial state parameter I_{ep}^0 > 1, indicating that ISPs are above BCSP, while a specimen is dense when I_{ep}^0 < 1, indicating that ISPs are below BCSP. The void-ratio-pressure state parameter I_{ep} approaches one as the specimen is sheared to critical state, where CSPs are on BCSP. Therefore, the void-ratio-pressure state parameter could describe the evolution of state-dependent behavior for crushable sands during the shearing process.

Friction Angle and Stress Ratio

The mobilized fraction angle ϕ_m is an important mechanical parameter for granular soils, which can be defined under triaxial compression condition as follows:

$$\sin\phi_m = \frac{3\eta}{6+\eta} \quad \textbf{(12)}$$

where the stress ratio η, the deviatoric stress q, and the mean effective stress p' under the triaxial condition can be expressed as:

$$\eta = \frac{q}{p'} \quad \textbf{(13a)}$$

$$q=\sigma_1'-\sigma_3' \quad \textbf{(13b)}$$

$$p'=(\sigma_1'+2\sigma_3')/3 \quad \textbf{(13c)}$$

The stress ratio η becomes the critical-state stress ratio M_{cs} when specimen is sheared to critical state.

Yielding Surface and Loading Unit Vector

The yielding surface of modified Cam-Clay (MCC) model proposed by Roscoe and Burland (1968) is adopted in this study:

$$f(p',q,p_0)=p'(1+\frac{\eta^2}{M_{cs}^2})-p_0=0 \quad \textbf{(14)}$$

where p_0 is the initial confining pressure.

The compression-related component (n_v^f) and shearing-related component (n_s^f) of the loading unit vector, which are normal to the MCC yielding surface, can be expressed as follows:

$$n_v^f=\frac{\frac{\partial f}{\partial p'}}{\sqrt{\left(\frac{\partial f}{\partial p'}\right)^2+\left(\frac{\partial f}{\partial q}\right)^2}}=\frac{\left(M_{cs}^2-\eta^2\right)}{\sqrt{\left(M_{cs}^2-\eta^2\right)^2+4\eta^2}} \quad \textbf{(15a)}$$

$$n_s^f=\frac{\frac{\partial f}{\partial q}}{\sqrt{\left(\frac{\partial f}{\partial p'}\right)^2+\left(\frac{\partial f}{\partial q}\right)^2}}=\frac{2\eta}{\sqrt{\left(M_{cs}^2-\eta^2\right)^2+4\eta^2}} \quad \textbf{(15b)}$$

Dilatancy and Plastic Flow Rule

Rowe (1962) proposed a stress-dilatancy relation for the uniform rods according to the minimum energy theory:

$$\sin\psi_m = \frac{\sin\phi_m - \sin\phi_{cs}}{1 - \sin\phi_m \sin\phi_{cs}} \quad \textbf{(16)}$$

where ϕ_{cs} is the critical-state friction angle and ψ_m is the mobilized dilatation angle. A modified Rowe stress-dilatancy equation was proposed by Xu and Song (2009) due to the difference in deformation mechanism and particle characteristics of actual soils as compared to the uniform rods, which is given as:

$$\sin\psi_m = d_0 \frac{\sin\phi_m - \sin\phi_{cs}}{1 - \sin\phi_m \sin\phi_{cs}} \quad \textbf{(17)}$$

where d_0 is a dilatancy parameter. In addition, Wan and Guo (1998) incorporated the void-ratio state parameter into the Rowe's stress-dilatancy equation to account for the state-dependent dilatancy behavior, which is expressed as:

$$\sin\psi_m = \frac{\sin\phi_m - \left(e/e_{cs}\right)^{\alpha} \sin\phi_{cs}}{1 - \left(e/e_{cs}\right)^{\alpha} \sin\phi_m \sin\phi_{cs}} \quad \textbf{(18)}$$

where α is a dilatancy parameter. Furthermore, Xiao et al. (2017) suggested a logically modified Rowe's stress-dilatancy equation by incorporating the void-ratio-pressure state parameter into the above two modifications, which can be given as:

$$\sin\psi_m = d_0 \frac{\sin\phi_m - \exp\left[\vartheta_d\left(I_{ep} - 1\right)\right]\sin\phi_{cs}}{1 - \exp\left[\vartheta_d\left(I_{ep} - 1\right)\right]\sin\phi_m \sin\phi_{cs}} \quad \textbf{(19)}$$

where ϑ_d is a dilatancy parameter.

A coefficient of dilatancy ratio S_d is defined as:

$$S_d = I_{ep}^{k_d} \quad \textbf{(20)}$$

where k_d is a dilatancy ratio parameter. It is noted that S_d meets the following requirement at critical state:

$$S_d\big|_{\eta=M_{cs},e=e_{cs}} = I_{ep}^{k_d} = 1^{k_d} = 1 \quad \textbf{(21)}$$

A new modification of Rowe's stress-dilatancy equation in this paper is defined as:

$$\sin\psi_m = d_0 \frac{\sin\phi_m - S_d \sin\phi_{cs}}{1 - S_d \sin\phi_m \sin\phi_{cs}} = d_0 \frac{\sin\phi_m - I_{ep}^{k_d} \sin\phi_{cs}}{1 - I_{ep}^{k_d} \sin\phi_m \sin\phi_{cs}} \quad \textbf{(22)}$$

The dilatancy d (by neglecting elastic strains) and the dilatation angle ψ_m at triaxial conditions are defined as:

$$d = -\frac{d\varepsilon_v^p}{d\varepsilon_s^p} = -\frac{3\,d\varepsilon_v / d\varepsilon_a}{3 - d\varepsilon_v / d\varepsilon_a} \quad \textbf{(23a)}$$

$$\sin\psi_m = -\frac{d\varepsilon_v / d\varepsilon_a}{2 - d\varepsilon_v / d\varepsilon_a} \quad \textbf{(23b)}$$

where $d\varepsilon_a$ and $d\varepsilon_v$ are axial and volumetric strain increments, respectively. Combination of **Eqs. (23a)** and **(23b)** gives:

$$d = \frac{6\sin\psi_m}{3 - \sin\psi_m} \quad \textbf{(24)}$$

Substituting **Eq. (22)** into **Eq. (24)** yields:

$$d = \frac{6d_0 \sin\phi_m - 6d_0 \sin\phi_{\mathrm{cs}} I_{ep}^{k_d}}{3 - d_0 \sin\phi_m - \sin\phi_{\mathrm{cs}}\left(3\sin\phi_m - d_0\right) I_{ep}^{k_d}} \quad \textbf{(25)}$$

The compression-related component (n_v^g) and shearing-related component (n_s^g) of the plastic flow unit vector can be defined as:

$$n_v^g = \frac{-d}{\sqrt{1+d^2}} \quad \textbf{(26a)}$$

$$n_s^g = \frac{1}{\sqrt{1+d^2}} \tag{26b}$$

Substitution of **Eq. (25)** into **Eq. (26)** yields:

$$n_v^g = \frac{-\dfrac{6d_0 \sin\phi_m - 6d_0 \sin\phi_{cs} I_{ep}^{k_d}}{3-d_0 \sin\phi_m - \sin\phi_{cs}\left(3\sin\phi_m - d_0\right) I_{ep}^{k_d}}}{\sqrt{1+\left[\dfrac{6d_0 \sin\phi_m - 6d_0 \sin\phi_{cs} I_{ep}^{k_d}}{3-d_0 \sin\phi_m - \sin\phi_{cs}\left(3\sin\phi_m - d_0\right) I_{ep}^{k_d}}\right]^2}} \tag{27a}$$

$$n_s^g = \frac{1}{\sqrt{1+\left[\dfrac{6d_0 \sin\phi_m - 6d_0 \sin\phi_{cs} I_{ep}^{k_d}}{3-d_0 \sin\phi_m - \sin\phi_{cs}\left(3\sin\phi_m - d_0\right) I_{ep}^{k_d}}\right]^2}} \tag{27b}$$

Bounding Stress Ratio and Plastic Modulus

A coefficient of bounding stress ratio S_b is defined as:

$$S_b = I_{ep}^{-k_b} \tag{28}$$

where k_b is a bounding stress-ratio parameter. It is noted that S_b meets the following requirement at critical state:

$$S_b\big|_{\eta=M_{cs}, e=e_{cs}} = I_{ep}^{-k_b} = 1^{-k_b} = 1 \tag{29}$$

Therefore, the bounding stress ratio M_b satisfies the following condition at critical state:

$$\begin{aligned} M_b\big|_{\eta=M_{cs}, e=e_{cs}} &= M_{cs} S_b = M_{cs} I_{ep}^{-k_b} \\ &= M_{cs} 1^{-k_b} = M_{cs} \end{aligned} \tag{30}$$

Based on **Eqs. (11)** and **(30)**, the state-dependent bounding stress ratio M_b considering the effect of particle breakage is given as:

$$M_b = M_{cs} \left\{ \frac{\dfrac{ep'}{e_{B0} - k_B \exp\left(\chi_B B_r\right) - \lambda \ln p'}}{\exp\left\{\dfrac{1}{\lambda}\left[e_{B0} - k_B \exp\left(\chi_B B_r\right) - e\right]\right\}} \right\}^{-k_b} \tag{31}$$

Equation (31) indicates that M_b is correlated to grain crushing. A breakage-state-dependent plastic modulus H_p can be expressed as a function of G_e, η and M_b:

$$\begin{aligned} H_p &= h_0 G_e \left(M_b - \eta\right) \Big/ \left(1+\eta\right)^4 \\ &= h_0 G_e \left(M_{cs} I_{ep}^{-k_b} - \eta\right) \Big/ \left(1+\eta\right)^4 \end{aligned} \tag{32}$$

where h_0 depends on confining pressure according to the tests on silica and coral sands and can be expressed as:

$$h_0 = \chi_h \left(\frac{p_0}{p_a}\right)^{-k_h} \tag{33}$$

where χ_h and k_h are pressure-dependent plastic modulus parameters.

Strain-Stress Relationships

Strain increments produced by stress increments can be expressed as the sum of elastic and plastic strain increments:

$$d\varepsilon_v = d\varepsilon_v^e + d\varepsilon_v^p \tag{34a}$$

$$d\varepsilon_s = d\varepsilon_s^e + d\varepsilon_s^p \tag{34b}$$

where $d\varepsilon_s$ is the total shear strain increment; $d\varepsilon_v^e$ is the elastic volumetric strain increment; $d\varepsilon_s^e$ is the elastic shear strain increment; and other strain increments have already been defined in previous Sections. In addition, the axial strain increment $d\varepsilon_a$ under the triaxial condition can be expressed as:

$$d\varepsilon_a = d\varepsilon_v / 3 + d\varepsilon_s \tag{35}$$

For simplicity, the elastic volumetric and shear strain increments can be expressed as:

$$d\varepsilon_v^e = dp' / K_e \tag{36a}$$

$$d\varepsilon_s^e = dq / \left(3G_e\right) \tag{36b}$$

where dp' and dq are the mean effective stress and deviatoric stress increments, respectively; K_e and

G_e are the elastic bulk modulus and elastic shear modulus, respectively. Hardin and Richart (1963) pointed out that G_e can be expressed as a function of the mean effective stress p' and void ratio e at the current state:

$$G_e = G_0 \frac{(2.97-e)^2}{1+e}\sqrt{p'p_a} \quad \textbf{(37)}$$

where p_a is the atmospheric pressure of 0.1 MPa; and G_0 is the elastic shearing modulus parameter. The elastic bulk modulus is usually expressed as a function of the elastic shear modulus G_e and Poisson's ratio υ:

$$\begin{aligned} K_e &= G_e \frac{2(1+\upsilon)}{3(1-2\upsilon)} \\ &= G_0\sqrt{p'p_a}\frac{(2.97-e)^2}{1+e}\frac{2(1+\upsilon)}{3(1-2\upsilon)} \end{aligned} \quad \textbf{(38)}$$

Based on a non-associated flow rule, the plastic strain increments ($d\varepsilon_v^p$ and $d\varepsilon_s^p$) is given as:

$$d\varepsilon_v^p = \frac{1}{H_p}\left(n_v^f dp' + n_s^f dq\right)n_v^g \quad \textbf{(39a)}$$

$$d\varepsilon_s^p = \frac{1}{H_p}\left(n_v^f dp' + n_s^f dq\right)n_s^g \quad \textbf{(39b)}$$

Substituting **Eqs. (31)**, **(33)** and **(37)** into **Eq. (32)** gives:

$$\begin{aligned} H_p &= h_1\left(\frac{p_0}{p_a}\right)^{k_h} G_0 \frac{(2.97-e)^2}{1+e}\frac{\sqrt{p'p_a}}{(1+\eta)^4}\times \\ &\left\{ M_{cs}\left\{\frac{\dfrac{ep'}{e_{B0}-k_B\exp(\chi_B B_r)-\lambda\ln p'}}{\exp\left[\dfrac{e_{B0}-k_B\exp(\chi_B B_r)-e}{\lambda}\right]}\right\}^{-k_b} - \eta \right\} \end{aligned} \quad \textbf{(40)}$$

Equation (40) indicates that the particle breakage can affect the plastic modulus. In addition, the plastic modulus H_p can also be used to capture the particle breakage-induced plastic strain under the isotropic compression condition.

Determinations of Model Parameters

The new model for crushable sand has fourteen material parameters, as listed in **Tables 1** and **2**, including two elastic parameters (G_0 and υ), five breakage-dependent critical state parameters (M_{cs}, λ, e_{B0}, k_B and χ_B), two breakage-energy parameters (χ_W and k_W), two dilatancy parameters (d_0 and k_d), one bounding stress-ratio parameter (k_b), and two plastic modulus parameters (χ_h and k_h). The values of breakage-energy parameters determined by Yu (2017a) and Yu (2018) are adopted in this study. The determinations of other model parameters are based on the methods used in previous studies (Li and Dafalias 2000; Xiao and Liu 2017). The values of two plastic modulus parameters can be determined by the plastic modulus calibrated from a series of triaxial tests under different confining pressures. **Table 1** lists values of initial state and model parameters and their changed values within a certain range to study their effects on the stress-strain relationships and evolution of particle breakage. **Table 2** lists the calibrated values of the model parameters from the test data by Yu (2017a) and Yu (2018).

Model Performances and Predictions

Variations of the initial state and model parameters listed in **Table 1** are applied to assess the model capability to simulate the evolution of stress, deformation, and particle breakage. **Figs. 4a-4d** show the effect of initial confining pressure p_0 on model predictions. The model can predict strain softening and volumetric expansion at a low confining pressure of 0.6 MPa, and strain hardening and volumetric contraction behavior at a high confining pressure of 1.2 MPa. An increase in confining pressure results in a significant increase in particle breakage, as shown in **Figs. 4c-4d**. Similarly, as shown in in **Figs. 5a-5b**, the transition from strain softening and volumetric expansion to strain hardening and volumetric contraction can be predicted with an increase in void ratio from 0.7 to 0.9. **Figs. 5c~5d** show that the influence of void ratio on particle breakage is less than that of confining pressure in **Figs. 4c-4d**. Meanwhile, an increase in initial elastic shearing modulus G_0 in **Figs. 6a-6d** can lead to an increase in strain softening, dilatancy and particle breakage. **Figs. 7a-7d** show that an increase in the parameter λ results in a great decrease in peak-state strength, a great increase in volumetric strain, and a neglectable change in particle breakage. The dilatancy parameter d_0 in **Figs. 8a-8d** mainly affects the maximum dilatancy and volumetric strain while the dilatancy parameter k_d in **Figs. 9a~9d** mainly influences the maximum dilatancy. **Figs. 10a-10d** show that an increase in bounding stress-ratio parameter k_b leads to a great increase in peak-state strength and maximum dilatancy, a great decrease in volumetric strain, and a slightly increase in particle breakage. The plastic modulus parameter h_0 in **Figs. 11a~11d** plays a similar role on peak-state strength, maximum dilatancy, volumetric strain, and particle breakage as the bounding stress-ratio parameter k_b.

Figures 12-19 describe the comparisons between model predictions and test data for silica sand from Yu (2017a) and coral sand from Yu (2018) with different values of initial state parameter I_{ep}^0. Model predictions and test data on the evolutions of stress ratio, volumetric strain, particle breakage and plastic work are shown in **Figs. 12-13** for silica sand at p_0 = 1 MPa with e_0 = 0.798 and 0.825, respectively. The difference in model predictions on the η - ε_a relationship with and without particle breakage is marginal whereas the prediction on the volumetric strain for the proposed model with particle breakage is larger than that without particle breakage. The proposed model prediction for test data with particle breakage is overall better than that without particle breakage, especially for a low void ratio of 0.798. For a high confining pressure, as shown in **Figs. 14-16**, the volumetric contraction is underestimated by the model without particle breakage at ε_a > 8% but well predicted by the proposed model with particle breakage. In addition, the evolution of particle breakage with respect to the axial strain or plastic work are well predicted by the proposed model with particle breakage.

As expected, coral sand with $e_0 = 0.798$ at $p_0 = 3$ MPa in **Fig. 17** exhibits more particle breakage than silica sand under the same condition in **Fig. 16**. In addition, the underestimation of volumetric strain predicted by the model without particle breakage becomes more obvious for coral sand in **Figs. 17-19**, whereas the proposed model with particle breakage can well capture the evolution of the stress ratio, volumetric strain and particle breakage, which would be attributed to the application of the BCSP, the corresponding void-ratio-pressure state parameter, and the breakage-state-dependent dilatancy and plastic modulus in the proposed model. Consequently, the proposed model can well capture the stress-strain relationship of crushable soils by the coupled influences of the contraction caused by particle breakage and dilatancy caused by particle rearrangement.

Discussion

In the triaxial test, the critical state of sand with particle breakage in the compression plane is a competition between the shrinkage due to particle crushing and the expansion due to particle rearrangement (Luzzani and Coop 2002; Hasanlourad et al. 2008). The developed model introduced the breakage-dependent void-ratio-pressure state parameter I_{ep} into dilatancy ratio and bounding stress ratio, which can reflect the state-dependent behaviors of crushable sand. As shown in **Figs. 20-21,** the state parameter I_{ep} is represented by a breakage-dependent state vertical wall (BSVW) that is formed by the projection of the predicted breakage-dependent deformation path to the BCSP. For the initial state parameter I_{ep}^0 smaller than one, as shown in **Fig. 20(a)**, the height of the BSVW approaches zero below the BCSP as the final critical state is gradually reached. For the initial state parameter I_{ep}^0 larger than one, as shown in **Fig. 20(b)**, the height of the BSVW approaches zero above the BCSP as the final critical state is gradually reached. For coral sand, as shown in **Figs. 21(b)-21(c)**, critical state is not reached at the axial strain of 0.2, as the height of the BSVW is not zero. **Figs. 18(b)** and **19(b)** also illustrate that the volumetric strain increment is still considerable, as the particle breakage continuously increases for coral sand at this condition.

Figures 22-23 present the evolutions of yielding surfaces, loading unit vector and plastic flow unit vector with particle breakage. The loading unit vector is always perpendicular to the yielding surface, whereas the plastic flow unit vector is not always perpendicular to the yielding surface. **Figs. 22(a)-22(b)** show that the plastic flow unit vector is approximately perpendicular to the yielding surface at its top point and close to the loading unit vector at the end of shearing process, which yields that the plastic volumetric strain increment is comparatively small. In contrast, **Figs. 23(a)-23(c)** show that the plastic flow unit vector is not perpendicular to the yielding surface at its top point, which illustrates that the plastic volumetric strain induced by particle breakage still increases at a considerable rate. These findings are in line with the model predictions as mentioned before.

It is significant for engineering applications to consider particle breakage and improve the predictions of the deformation and strength of geomaterials, especially for the infrastructures sustained high stress and/or large displacement, e.g. pile-driven engineering, high rockfill dam, etc. The framework in this study can provide a theoretical basis to analyze the stability of infrastructure engineering involving particle breakage when this model is implemented into finite element method or material point method, which will be investigated in future.

Conclusions

A constitutive model was proposed for sands under high pressure by considering the effect of grain crushing on strength and deformation. The major conclusions of this research are summarized below:

(1) Based on the concept of the breakage-dependent critical state surface (BCSP), the void-ratio-pressure state parameter is adopted to reflect the effect of particle breakage. The evolution of the current state point with the BCSP during shearing process demonstrates the capability of the proposed state parameter in reflecting the effects of particle breakage on state-dependent behaviors of sands under high pressure.

(2) The breakage-dependent void-ratio-pressure state parameter is incorporated into Rowe's stress dilatancy equation, bounding stress ratio and plastic modulus to reflect the influence of particle breakage on the state-dependent characteristics. Based on the bounding surface plasticity framework and the non-associated flow rule, a constitutive model considering the state-dependent and particle breakage is established for silica and coral sands under high pressure.

(3) Effects of model parameters on the stress-strain relationship and evolution of particle breakage are also investigated. Based on the comparisons between model predictions and test results, the proposed model can better capture the evolution of particle breakage and its effects on the stress-strain relationship, which is mainly attributed to the use of BCSP and breakage-dependent void-ratio-pressure state parameter.

Data Availability

All data, models, and code generated or used during the study appear in the submitted article.

Acknowledgments

The authors would like to acknowledge the financial support from the National Nature Science Foundation of China (Grant No. 51922024, Grant No. 41831282, Grant No. 51978104, and Grant No.

51678094) and Natural Science Foundation of Chongqing, China (Grant No. cstc2019jcyjjqX0014).

Notations

The following symbols are used in this paper:

I_{ep} =Void-ratio-pressure state parameter;

I_{ep}^{0} =Initial void-ratio-pressure state parameter;

p_0 =Initial confining pressure (unit: MPa);

p' =Mean effective stress (unit: MPa);

q =Deviatoric stress (unit: MPa);

p'_{cs} =Critical-state mean effective stress (unit: MPa);

p_a =Atmospheric pressure (unit: MPa);

$\sigma_1^{'}$ and $\sigma_3^{'}$ =Maximum and minimum principle stress, respectively (unit: MPa);

dp' and dq = Mean effective stress increment and deviatoric stress increment, respectively (unit: MPa);

$\mathrm{d}\varepsilon_a$ =Axial strain increment (unit: %);

$d\varepsilon_v$ and $d\varepsilon_s$ =Volumetric strain and shear strain increments, respectively (unit: %);

$d\varepsilon_v^e$ and $d\varepsilon_s^e$ =Elastic volumetric and shear strain increments, respectively (unit: %);

$d\varepsilon_v^p$ and $d\varepsilon_s^p$ =Plastic volumetric and shear strain increments, respectively (unit: %);

n_v^f and n_s^f =Compression-related and shearing-related components of the loading unit vector, respectively;

n_v^g and n_s^g =Compression-related and shearing-related components of the plastic-flow unit vector, respectively;

η =Stress ratio;

ϕ_{cs} =Critical state friction angle (unit: degree);

ϕ_m and ψ_m =Mobilized friction angle and dilatation angle, respectively (unit: degree);

e =Current void ratio;

e_0 =Initial void ratio;

e_{cs} =Critical state void ratio;

e_{cs0} =Initial critical state void ratio;

λ, e_{B0}, k_B and χ_B =Breakage-dependent critical-state parameters;

M_{cs} =Critical state stress ratio;

M_b =Bounding stress ratio;

S_b =Coefficients of bounding stress ratio;

k_b = Bounding stress-ratio parameter;

B_r =Relative breakage index (unit: %);

d =Dilatancy;

S_d =Coefficient of dilatancy ratio;

d_0, α ϑ_d, and k_d =Dilatancy parameters;

W_p =Plastic work (unit: MJ/m^3);

χ_W =Breakage-energy parameter (unit: MJ/m^3);

k_W =Breakage-energy parameter;

K_e and G_e =Elastic bulk modulus and elastic shear modulus, respectively;

G_0 =Elastic shear modulus parameter;

υ =Poisson's ratio;

H_p =Plastic modulus;

h_0 = Pressure-dependent plastic modulus parameter; and

χ_h and k_h =Plastic modulus parameters.

References:

Alonso, E. E., Romero, E. E., and Ortega, E. (2016). "Yielding of rockfill in relative humidity-controlled triaxial experiments." *Acta Geotechnica*, 11(3), 455-477.

Altuhafi, F. N., Jardine, R. J., Georgiannou, V. N., and Moinet, W. W. (2018). "Effects of particle breakage and stress reversal on the behaviour of sand around displacement piles." *Géotechnique*, 68(6), 546-555.

Bandini, V., and Coop, M. R. (2011). "The influence of particle breakage on the location of the critical state line of sands." *Soils Found.*, 51(4), 591-600.

Bardet, J. P. (1986). "Bounding surface plasticity model for sands." *J. Eng. Mech*, 112(11), 1198-1217.

Been, K., and Jefferies, M. G. (1985). "A state parameter for sands." *Geotechnique*, 35(2), 99-112.

Been, K., Jefferiest, M. G., and Hachey, J. (1991). "The critical state of sands." *Geotechnique*, 41(3), 365-381.

Bolton, M. D. (1986). "The strength and dilatancy of sands." *Geotechnique*, 36(1), 65-78.

Chang, D., Lai, Y., and Gao, J. (2019). "An investigation on the constitutive response of frozen saline coarse sandy soil based on particle breakage and plastic shear mechanisms." *Cold Reg. Sci. Technol.*, 159(March), 94-105.

Chen, Q., Indraratna, B., Carter, J. P., and Nimbalkar, S. (2016). "Isotropic-kinematic hardening model for coarse granular soils capturing particle breakage and cyclic loading under triaxial stress space." *Can. Geotech. J.*, 53(4), 646-658.

Chen, W.-B., Liu, K., Yin, Z.-Y., and Yin, J.-H. (2020). "Crushing and flooding effects on one-dimensional time-dependent behaviors of a granular soil." *Int. J. Geomech.*, 20(2), 04019156.

Chiu, C. F., and Fu, X. J. (2008). "Interpreting undrained instability of mixed soils by equivalent intergranular state parameter." *Géotechnique*, 58(9), 751-755.

Chu, J., and Leong, W. K. (2002). "Effect of fines on instability behaviour of loose sand." *Geotechnique*, 52(10), 751-755.

Chu, J., and Wanatowski, D. (2008). "Instability conditions of loose sand in plane strain." *J. Geotech. Geoenviron. Eng.*, 134(1), 136-142.

Chu, J., and Wanatowski, D. (2009). "Effect of loading mode on strain softening and instability behavior of sand in plane-strain tests." *J. Geotech. Geoenviron. Eng.*, 135(1), 108-120.

Ciantia, M. O., Arroyo, M., O'Sullivan, C., Gens, A., and Liu, T. (2019). "Grading evolution and critical state in a discrete numerical model of Fontainebleau sand." *Géotechnique*, 69(1), 1-15.

Ciantia, M. O., and O'Sullivan, C. (2020). "Calculating the state parameter in crushable sands." *Int. J. Geomech.*

Cil, M. B., Hurley, R. C., and Graham-Brady, L. (2020). "Constitutive Model for Brittle Granular Materials Considering Competition between Breakage and Dilation." *J. Eng. Mech*, 146(1), 04019110.

Coop, M. R., Sorensen, K. K., Bodas Freitas, T., and Georgoutsos, G. (2004). "Particle breakage during shearing of a carbonate sand." *Geotechnique*, 54(3), 157-163.

Dafalias, Y. F., and Popov, E. P. (1976). "Plastic internal variables formalism of cyclic plasticity." *Journal of Applied Mechanics*, 43(4), 645-651.

Daouadji, A., and Hicher, P.-y. (2010). "An enhanced constitutive model for crushable granular materials." *Int. J. Numer. Anal. Met.*, 34(6), 555-580.

Daouadji, A., Hicher, P.-Y., and Rahma, A. (2001). "An elastoplastic model for granular materials taking into account grain breakage." *European Journal of Mechanics - A/Solids*, 20(1), 113-137.

Desai, C. S. (2000). "Evaluation of liquefaction using disturbed state and energy approaches." *J. Geotech. Geoenviron. Eng.*, 126(7), 618-631.

Einav, I. (2007). "Breakage mechanics-Part I: Theory." *J. Mech. Phys. Solids*, 55(6), 1274-1297.

Fukuoka, H., Sassa, K., and Wang, G. (2006). "Influence of shear speed and normal stress on the shear behavior and shear zone structure of granular materials in naturally drained ring shear tests." *Landslides*, 4(1), 63-74.

Gajo, A., and Muir Wood, D. (1999). "Severn-Trent sand : a kinematic-hardening constitutive model : the q-p formulation." *Geotechnique*, 49(5), 595-614.

Ganju, E., Han, F., Prezzi, M., Salgado, R., and Pereira, J. S. (2020). "Quantification of displacement and particle crushing around a penetrometer tip." *Geoscience Frontiers*, 11(2), 389-399.

Ghafghazi, M., Shuttle, D. A., and DeJong, J. T. (2014). "Particle breakage and the critical state of sand." *Soils Found.*, 54(3), 451-461.

Hagerty, M. M., Hite, D. R., Ullrich, C. R., and Hagerty, D. J. (1993). "One-dimensional high-pressure compression of granular media." *J. Geotech. Eng.*, 119(1), 1-18.

Hardin, B. O. (1985). "Crushing of soil particles." *J. Geotech. Eng.*, 111(10), 1177-1192.

Hardin, B. O., and Richart, F. E. (1963). "Elastic wave velocities in granular soils." *J. Soil Mech. Found.*, 89(1), 33-66.

Hasanlourad, M., Salehzadeh, H., and Shahnazari, H. (2008). "Dilation and particle breakage effects on the shear strength of calcareous sands based on energy aspects." *International Journal of Civil Engineerng*, 6(2), 108-119.

Heitor, A., Indraratna, B., Kaliboullah, C. I., Rujikiatkamjorn, C., and McIntosh, G. W. (2016). "Drained and Undrained Shear Behavior of Compacted Coal Wash." *J. Geotech. Geoenviron. Eng.*, 142(5), 04016006.

Hiroshi, F., Kyoji, S., Gonghui, W., and Ryo, S. (2006). "Observation of shear zone development in ring-shear apparatus with a transparent shear box." *Landslides*, 3(3), 239-251.

Hu, W., Yin, Z., Dano, C., and Hicher, P.-Y. (2011). "A constitutive model for granular materials considering grain breakage." *Sci. China Tech. Sci.*, 54(8), 2188-2196.

Huang, J., Xu, S., Yi, H., and Hu, S. (2014). "Size effect on the compression breakage strengths of glass particles." *Power Technology*, 268(1), 86-94.

Huang, J. Y., Hu, S. S., Xu, S. L., and Luo, S. N. (2017). "Fractal crushing of granular materials under confined compression at different strain rates." *Int. J. Impact. Eng.*, 106(August), 259-265.

Hyodo, M., Wu, Y., Aramaki, N., and Nakata, Y. (2016). "Undrained monotonic and cyclic shear response and particle crushing of silica sand at low and high pressures." *Can. Geotech. J.*, 54(2), 207-218.

Indraratna, B., Ngo, T. N., and Rujikiatkamjorn, C. (2020). "Performance of ballast influenced by deformation and degradation: laboratory testing andnumerical modeling." *Int. J. Geomech.*, 20(1), 04019138.

Indraratna, B., and Salim, W. (2002). "Modelling of particle breakage of coarse aggregates incorporating strength and dilatancy." *Geotechnical Engineering*, 155(4), 243-252.

Indraratna, B., Sun, Q. D., and Nimbalkar, S. (2015). "Observed and predicted behaviour of rail ballast under monotonic loading capturing particle breakage." *Can. Geotech. J.*, 52(1), 73-86.

Jefferies, M. G. (1993). "Nor-Sand: a simple critical state model for sand." *Geotechnique*, 43(1), 91-103.

Jia, Y., Xu, B., Chi, S., Xiang, B., and Zhou, Y. (2017). "Research on the Particle Breakage of Rockfill Materials during Triaxial Tests " *Int. J. Geomech.*, 17(10), 04017085.

Kan, M. E., and Taiebat, H. (2014). "A bounding surface plasticity model for highly crushable granular materials." *Soils Found.*, 54(6), 1188-1201.

Kan Mojtaba, E., Taiebat Hossein, A., and Khalili, N. (2014). "Simplified Mapping Rule for Bounding Surface Simulation of Complex Loading Paths in Granular Materials." *Int. J. Geomech.*, 14(2), 239-253.

Kikumoto, M., Muir Wood, D., and Russell, A. (2010). "Particle crushing and deformation behaviour." *Soils Found.*, 50(4), 547-563.

Kuwajima, K., Hyodo, M., and Hyde, A. F. L. (2009). "Pile bearing capacity factors and soil crushabiity." *J. Geotech. Geoenviron. Eng.*, 135(7), 901-913.

Lade, P. V., Liggio, C. D., and Nam, J. (2009). "Strain Rate, Creep, and Stress Drop-Creep Experiments on Crushed Coral Sand." *J. Geotech. Geoenviron. Eng.*, 135(7), 941-941.

Lade, P. V., Yamamuro, J. A., and Bopp, P. A. (1996). "Significance of particle crushing in granular materials." *J. Geotech. Eng.*, 122(4), 309-316.

Lashkari, A. (2016). "Prediction of flow liquefaction instability of clean and silty sands." *Acta Geotechnica*, 11(5), 987-1014.

Lashkari, A., and Yaghtin, M. S. (2018). "Sand flow liquefaction instability under shear–volume coupled strain paths." *Géotechnique*, 68(11), 1002-1024.

Li, X. S., and Dafalias, Y. F. (2000). "Dilatancy for cohesionless soils." *Geotechnique*, 50(4), 449-460.

Ling, H. I., and Yang, S. (2006). "Unified sand model based on the critical state and generalized plasticity." *J. Eng. Mech*, 132(12), 1380-1391.

Liu, G.-Y., Xu, W.-J., Sun, Q.-C., and Govender, N. (2019). "Study on the particle breakage of ballast based on a GPU accelerated discrete element method." *Geoscience Frontiers*, 11(2), 461-471.

Liu, H., Zeng, K., and Zou, Y. (2020). "Particle breakage of calcareous sand and its correlation with input energy." *Int. J. Geomech.*, 20(2), 04019151.

Liu, H., and Zou, D. (2013). "Associated generalized plasticity framework for modeling gravelly soils considering particle breakage." *J. Eng. Mech*, 139(5), 606-615.

Liu, J., Zou, D., Kong, X., and Liu, H. (2016). "Stress-dilatancy of Zipingpu gravel in triaxial compression tests." *Sci. China Tech. Sci.*, 59(2), 214-224.

Liu, M., and Gao, Y. (2017). "Constitutive modeling of coarse-grained materials incorporating the effect of particle breakage on critical state behavior in a framework of generalized plasticity." *Int. J. Geomech.*, 17(5), 04016113.

Lobo-Guerrero, S., and Vallejo, L. (2006). "Modeling granular crushing in ring shear tests: experimental and numerical analyses." *Soils Found.*, 46(2), 147-157.

Luzzani, L., and Coop, M. R. (2002). "On the relationship between particle breakage and the critical state of sands." *Soils Found.*, 42(2), 71-82.

Man, S., and Chik-Kwong Wong, R. (2017). "Compression and crushing behavior of ceramic proppants and sand under high stresses." *J. Petrol. Sci. Eng.*, 158(September), 268-283.

Mao, W., Aoyama, S., and Towhata, I. (2019). "A study on particle breakage behavior during pile penetration process using acoustic emission source location." *Geoscience Frontiers*, 11(2), 413-427.

Mao, W., Hamaguchi, H., and Koseki, J. (2020). "Discrimination of particle breakage below pile tip after model pile penetration in sand using image analysis." *Int. J. Geomech.*, 20(1), 04019142.

Mao, W., Yang, Y., Lin, W., Aoyama, S., and Towhata, I. (2018). "High Frequency Acoustic Emissions Observed during Model Pile Penetration in Sand and Implications for Particle Breakage Behavior." *Int. J. Geomech.*, 18(11), 04018143.

McDowell, G. R., and Amon, A. (2000). "The application of Weibull statistics to the fracture of soil particles." *Soils Found.*, 40(5), 133-141.

McDowell, G. R., and Bolton, M. D. (1998). "On the micromechanics of crushable aggregates." *Geotechnique*, 48(5), 667-679.

McDowell, G. R., Bolton, M. D., and Robertson, D. (1996). "The fractal crushing of granular materials." *J. Mech. Phys. Solids*, 44(12), 2079-2102.

Miao, G., and Airey, D. (2013). "Breakage and ultimate states for a carbonate sand." *Geotechnique*, 63(14), 1221-1229.

Muir Wood, D., Belkheir, K., and Liu, D. F. (1994). "Strain softening and state parameter for sand modelling." *Geotechnique*, 44(2), 335-339.

Muir Wood, D., and Maeda, K. (2008). "Changing grading of soil: effect on critical states." *Acta Geotechnica*, 3(1), 3-14.

Mun, W., and McCartney, J. S. (2017). "Roles of particle breakage and drainage in the isotropic compression of sand to high pressures." *J. Geotech. Geoenviron. Eng.*, 143(10), 04017071.

Nakata, Y., Hyde, A. F. L., Hyodo, M., and Murata, H. (1999). "A probabilistic approach to sand particle crushing in the triaxial test." *Geotechnique*, 49(5), 567-583.

Nakata, Y., Hyodo, M., Hyde, A. F. L., Kato, Y., and Murata, H. (2001). "Microscopic Particle Crushing of Sand Subjected to High Pressure One-Dimensional Compression." *Soils Found.*, 41(1), 69-82.

Ning, F., Liu, J., Kong, X., and Zou, D. (2020). "Critical state and grading evolution of rockfill material under different triaxial compression tests." *Int. J. Geomech.*, 20(2), 04019154.

Omidvar, M., Iskander, M., and Bless, S. (2012). "Stress-strain behavior of sand at high strain rates." *Int. J. Impact. Eng.*, 49, 192-213.

Ovalle, C., Dano, C., Hicher, P.-y., and Cisternas, M. (2015). "Experimental framework for evaluating the mechanical behavior of dry and wet crushable granular materials based on the particle breakage ratio." *Can. Geotech. J.*, 52(5), 587-598.

Ovalle, C., and Hicher, P.-Y. (2019). "Modeling the effect of wetting on the mechanical behavior of crushable granular materials." *Geoscience Frontiers*, 11(2), 487-494.

Pan, J., Jiang, J., Cheng, Z., Xu, H., and Zuo , Y. (2020). "Large-scale true triaxial test on stress-strain and strength properties of rockfill." *Int. J. Geomech.*, 20(1), 04019146.

Parab, N. D., Guo, Z., Hudspeth, M. C., Claus, B. J., Fezzaa, K., Sun, T., and Chen, W. W. (2017). "Fracture mechanisms of glass particles under dynamic compression." *Int. J. Impact. Eng.*, 106, 146-154.

Rabbi, A. T. M. Z., Rahman, M. M., and Cameron, D. (2019). "Critical State Study of Natural Silty Sand Instability under Undrained and Constant Shear Drained Path." *Int. J. Geomech.*, 19(8), 04019083.

Roscoe, K. H., and Burland, J. B. (1968). "On the generalised stress–strain behaviour of 'wet' clay." *Engineering plasticity*, J. Heyman, and F. A. Leckie, eds., Cambridge University Press, Cambridge, 535-609.

Rowe, P. W. (1962). "The stress-dilatancy relation for static equilibrium of an assembly of particles in contact." *Proc. R. Soc. Lond. A*, 269(1339), 500-527.

Russell, A. R., and Khalili, N. (2004). "A bounding surface plasticity model for sands exhibiting particle crushing." *Can. Geotech. J.*, 41(6), 1179-1192.

Sadrekarimi, A., and Olson, S. M. (2010). "Particle damage observed in ring shear tests on sands." *Can. Geotech. J.*, 47(5), 497-515.

Sadrekarimi, A., and Olson, S. M. (2011a). "Critical state friction angle of sands." *Géotechnique*, 61(9), 771-783.

Sadrekarimi, A., and Olson, S. M. (2011b). "Yield strength ratios, critical strength ratios, and brittleness of sandy soils from laboratory tests." *Can. Geotech. J.*, 48(3), 493-510.

Salgado, R., Bandini, P., and Karim, A. (2000). "Shear strength and stiffness of silty sand." *J. Geotech. Geoenviron. Eng.*, 126(5), 451-462.

Salim, W., and Indraratna, B. (2004). "A new elastoplastic constitutive model for coarse granular aggregates incorporating particle breakage." *Can. Geotech. J.*, 41(4), 657-671.

Suescun-Florez, E., Omidvar, M., Iskander, M., and Bless, S. (2015). "Review of High Strain Rate Testing of Granular Soils." *Geotech. Test. J.*, 38(4), 511-536.

Sun, Q., Indraratna, B., and Nimbalkar, S. (2015). "Deformation and Degradation Mechanisms of Railway Ballast under High Frequency Cyclic Loading." *J. Geotech. Geoenviron. Eng.*, 142(1), 04015056.

Sun, Y., Gao, Y., and Shen, Y. (2019). "Mathematical aspect of the state-dependent stress–dilatancy of granular soil under triaxial loading." *Geotechnique*, 69(2), 158-165.

Sun, Y., Gao, Y., Song, S., and Chen, C. (2020). "Three-Dimensional State-Dependent Fractional Plasticity Model for Soils." *Int. J. Geomech.*, 20(2), 04019161.

Tarantino, A., and Hyde, A. F. L. (2005). "An experimental investigation of work dissipation in crushable materials." *Geotechnique*, 55(8), 575-584.

Tengattini, A., Das, A., and Einav, I. (2016). "A constitutive modelling framework predicting critical state in sand undergoing crushing and dilation." *Geotechnique*, 66(9), 695-710.

Tong, C.-X., Burton, G. J., Zhang, S., and Sheng, D. (2020). "Particle breakage of uniformly graded carbonate sands in dry/wet condition subjected to compression/shear tests." *Acta Geotechnica*, In press.

Ueng, T. S., and Chen, T. J. (2000). "Energy aspects of particle breakage in drained shear of sands." *Geotechnique*, 50(1), 65-72.

Valdes, J. R., and Koprulu, E. (2007). "Characterization of Fines Produced by Sand Crushing." *J. Geotech. Geoenviron. Eng.*, 133(12), 1626-1630.

Varadarajan, A., Sharma, K. G., Abbas, S. M., and Dhawan, A. K. (2006). "Constitutive model for rockfill materials and determination of material constants." *Int. J. Geomech.*, 6(4), 226-237.

Varadarajan, A., Sharma, K. G., Venkatachalam, K., and Gupta, A. K. (2003). "Testing and modeling two rockfill materials." *J. Geotech. Geoenviron. Eng.*, 129(3), 206-206.

Wafid Agung, M., Sassa, K., Fukuoka, H., and Wang, G. (2004). "Evolution of Shear-Zone Structure in Undrained Ring-Shear Tests." *Landslides*, 1(2), 101-112.

Wan, R. G., and Guo, P. J. (1998). "A simple constitutive model for granular soils: Modified stress-dilatancy approach." *Comput. Geotech.*, 22(2), 109-133.

Wang, G., Wang, Z., Ye, Q., and Wei, X. (2020). "Particle breakage and deformation behavior of a carbonate sand under drained and undrained triaxial compression." *Int. J. Geomech.*, 20(3), 04020012.

Wang, X., Jiao, Y., Wang, R., Hu, M., Meng, Q., and Tan, F. (2011). "Engineering characteristics of the calcareous sand in Nansha Islands, South China Sea." *Eng. Geol.*, 120(1-4), 40-47.

Wang, Z. L., Dafalias, Y. F., Li, X. S., and Makdisi, F. I. (2002). "State pressure index for modeling sand behavior." *J. Geotech. Geoenviron. Eng.*, 128(6), 511-519.

Wei, H., Tao, Z., He, J., Meng, Q., and Wang, X. (2018). "Evolution of Particle Breakage for Calcareous Sands during Ring Shear Tests." *Int. J. Geomech.*, 18(2), 04017153.

Wei, X., and Yang, J. (2019). "A critical state constitutive model for clean and silty sand." *Acta Geotechnica*, 14(2), 329-345.

Wu, Y., Yamamoto, H., Cui, J., and Cheng, H. Y. (2020). "Influence of load mode on particle crushing characteristics of silica sand at high stresses." *Int. J. Geomech.*, 20(3), 04019194.

Xiao, Y., Chen, H., Stuedlein, A. W., Evans, T. M., Chu, J., Cheng, L., Jiang, N., Lin, H., Liu, H., and Aboel-Naga, H. M. (2020). "Restraint of Particle Breakage by Biotreatment Method." *J. Geotech. Geoenviron. Eng.*, 146(11), 04020123.

Xiao, Y., and Liu, H. (2017). "Elastoplastic constitutive model for rockfill materials considering particle breakage." *Int. J. Geomech.*, 17(1), 04016041.

Xiao, Y., Liu, H., Chen, Y., and Jiang, J. (2014). "Bounding surface plasticity model incorporating the state pressure index for rockfill materials." *J. Eng. Mech*, 140(11), 04014087.

Xiao, Y., Long, L., Evans, T. M., Zhou, H., Liu, H., and Stuedlein, A. W. (2019a). "Effect of Particle Shape on Stress-Dilatancy Responses of Medium-Dense Sands." *J. Geotech. Geoenviron. Eng.*, 145(2), 04018105.

Xiao, Y., Sun, Y., Yin, F., Liu, H., and Xiang, J. (2017). "Constitutive modeling for transparent granular soils." *Int. J. Geomech.*, 17(7), 04016150.

Xiao, Y., Yuan, Z., Chu, J., Liu, H., Huang, J., Luo, S. N., Wang, S., and Lin, J. (2019b). "Particle breakage and energy dissipation of carbonate sands under quasi-static and dynamic compression." *Acta Geotechnica*, 14(6), 1741-1755.

Xu, M., and Song, E. (2009). "Numerical simulation of the shear behavior of rockfills." *Comput. Geotech.*, 36(8), 1259-1264.

Yamamuro, J. A., Bopp, P. A., and Lade, P. V. (1996). "One-dimensional compression of sands at high pressures." *J. Geotech. Geoenviron. Eng.*, 122(2), 147-154.

Yang, J., and Li, X. S. (2004). "State-Dependent Strength of Sands from the Perspective of Unified Modeling." *J. Geotech. Geoenviron. Eng.*, 130(2), 186-198.

Yang, Z. X., Xu, T. T., and Li, X. S. (2019). "J2-deformation type model coupled with state dependent dilatancy." *Comput. Geotech.*, 105(January), 129-141.

Yao, Y. P., Sun, D. A., and Luo, T. (2004). "A critical state model for sands dependent on stress and density." *Int. J. Numer. Anal. Met.*, 28(4), 323-337.

Yin, Z., Hicher, P., Dano, C., and Jin, Y. (2017). "Modeling Mechanical Behavior of Very Coarse Granular Materials." *J. Eng. Mech*, 143(1), C4016006.

Yu, F. (2017a). "Characteristics of particle breakage of sand in triaxial shear." *Powder Technol.*, 320(October), 656-667.

Yu, F. (2017b). "Particle breakage and the drained shear behavior of sands." *Int. J. Geomech.*, 17(8), 04017041.

Yu, F. (2018). "Particle breakage in triaxial shear of a coral sand." *Soils Found.*, 58(4), 866-880.

Yu, F. (2019). "Influence of particle breakage on behavior of coral sands in triaxial tests." *Int. J. Geomech.*, 19(12), 04019131.

Yu, H. S. (1998). "CASM: A unified state parameter model for clay and sand." *Int. J. Numer. Anal. Met.*, 22(8), 621-653.

Zhang, C., Nguyen, G. D., and Einav, I. (2013). "The end-bearing capacity of piles penetrating into crushable soils." *Geotechnique*, 63(5), 341-354.

Zhang, J., and Luo, M. (2020). "Dilatancy and critical state of calcareous sand incorporating particle breakage." *Int. J. Geomech.*, 20(4), 04020030.

Zhang, X., and Baudet, B. A. (2013). "Particle breakage in gap-graded soil." *Geotech. Lett.*, 3(2), 72-77.

Zhang, Y., Buscarnera, G., and Einav, I. (2016). "Grain size dependence of yielding in granular soils interpreted using fracture mechanics, breakage mechanics and Weibull statistics." *Geotechnique*, 66(2), 149-160.

Zheng, W., and Tannant, D. (2016). "Frac sand crushing characteristics and morphology changes under high compressive stress and implications for sand pack permeability." *Can. Geotech. J.*, 53(9), 1412-1423.

Table 1. Values of initial state and model parameters for model presentations

Initial and material parameters	Basic values	Changed values
p_0 (MPa)	0.8	0.6, 1.2
e_0	0.8	0.7, 0.9
G_0	80	40, 160
υ	0.25	-
χ_W	7.847	-
k_W	1.686	-
λ	0.1	0.09, 0.11
e_{cs0}	1.598	-
k_B	0. 046	-
χ_B	5.698	-
d_0	1.2	0.6, 2.4
k_d	0.2	0.1, 0.4
k_b	0.4	0.2, 0.8
h_0	10	5, 20

Table 2. Values of model parameters of silica sand and coral sand for model simulations

Material parameters	Silica sand	Coral sand
G_0	86.4	87.2
υ	0.25	0.25
M_{cs}	1.36	1.32
χ_W	7.847	4.820
k_W	1.686	3.228
λ	0.10	0.10
e_{B0}	1.598	1.850
k_B	0.046	0.302
χ_B	5.698	2.0408
d_0	1.52	1.20
k_d	0.13	0.25
k_b	0.15	0.12
χ_h	904.0	613.6
k_h	1.45	1.16

Figure Caption List:

Fig. 1. (Color) BCSL and state parameter in the compression plane: (a and b) silica sand; and (c and d) coral sand

Fig. 2. (Color) BCSL and state parameter in three-dimensional e - B_r - p' space: (a and b) silica sand; and (c) coral sand.

Fig. 3. (Color) BCSL and state parameter in three-dimensional e - W_p - p' space: (a and b) silica sand; and (c) coral sand.

Fig. 4. (Color) Influence of p_0 on model performance: (a-d) η - ε_a, ε_v - ε_a, B_r - ε_a and B_r - ε_v planes, respectively.

Fig. 5. (Color) Influence of e_0 on model performance: (a-d) η - ε_a, ε_v - ε_a, B_r - ε_a and B_r - ε_v planes, respectively.

Fig. 6. (Color) Influence of G_0 on model performance: (a-d) η - ε_a, ε_v - ε_a, B_r - ε_a and B_r - ε_v planes, respectively.

Fig. 7. (Color) Influence of λ on model performance: (a-d) η - ε_a, ε_v - ε_a, B_r - ε_a and B_r - ε_v planes, respectively.

Fig. 8. (Color) Influence of d_0 on model performance: (a-d) η - ε_a, ε_v - ε_a, B_r - ε_a and B_r - ε_v planes, respectively.

Fig. 9. (Color) Influence of k_d on model performance: (a-d) η - ε_a, ε_v - ε_a, B_r - ε_a and B_r - ε_v planes, respectively.

Fig. 10. (Color) Influence of k_b on model performance: (a-d) η - ε_a, ε_v - ε_a, B_r - ε_a and B_r - ε_v planes, respectively.

Fig. 11. (Color) Influence of h_0 on model performance: (a-d) η - ε_a, ε_v - ε_a, B_r - ε_a and B_r - ε_v planes, respectively.

Fig. 12. (Color) Predictions for silica sand at I_{ep}^0 = 0.55: (a-d) η - ε_a, ε_v - ε_a, B_r - ε_a and B_r - W_p planes, respectively.

Fig. 13. (Color) Predictions for silica sand at I_{ep}^0 = 0.67: (a-d) η - ε_a, ε_v - ε_a, B_r - ε_a and B_r - W_p planes, respectively.

Fig. 14. (Color) Predictions for silica sand at I_{ep}^0 = 1.08: (a-d) η - ε_a, ε_v - ε_a, B_r - ε_a and B_r - W_p planes, respectively.

Fig. 15. (Color) Predictions for silica sand at I_{ep}^0 = 1.25: (a-d) η - ε_a, ε_v - ε_a, B_r - ε_a and B_r - W_p planes, respectively.

Fig. 16. (Color) Predictions for silica sand at I_{ep}^0 = 1.72: (a-d) η - ε_a, ε_v - ε_a, B_r - ε_a and B_r - W_p planes, respectively.

Fig. 17. (Color) Predictions for coral sand at I_{ep}^0 = 1.92: (a-d) η - ε_a, ε_v - ε_a, B_r - ε_a and B_r - W_p planes, respectively.

Fig. 18. (Color) Predictions for coral sand at I_{ep}^0 = 4.29: (a-d) η - ε_a, ε_v - ε_a, B_r - ε_a and B_r - W_p planes, respectively.

Fig. 19. (Color) Predictions for coral sand at I_{ep}^0 = 7.8: (a-d) η - ε_a, ε_v - ε_a, B_r - ε_a and B_r - W_p planes, respectively.

Fig. 20. (Color) Evolution of state vertical wall for silica sand: (a-c) p_0 = 1, 2 and 3 MPa, respectively.

Fig. 21. (Color) Evolution of state vertical wall for coral sand: (a-c) e_0 = 0.798, 0.870 and 0.924, respectively.

Fig. 22. (Color) Evolution of loading and plastic flow unit vectors: (a-c) p_0 = 1, 2 and 3 MPa, respectively.

Fig. 23. (Color) Evolution of loading and plastic flow unit vectors: (a-c) e_0 = 0.798, 0.870 and 0.924, respectively.

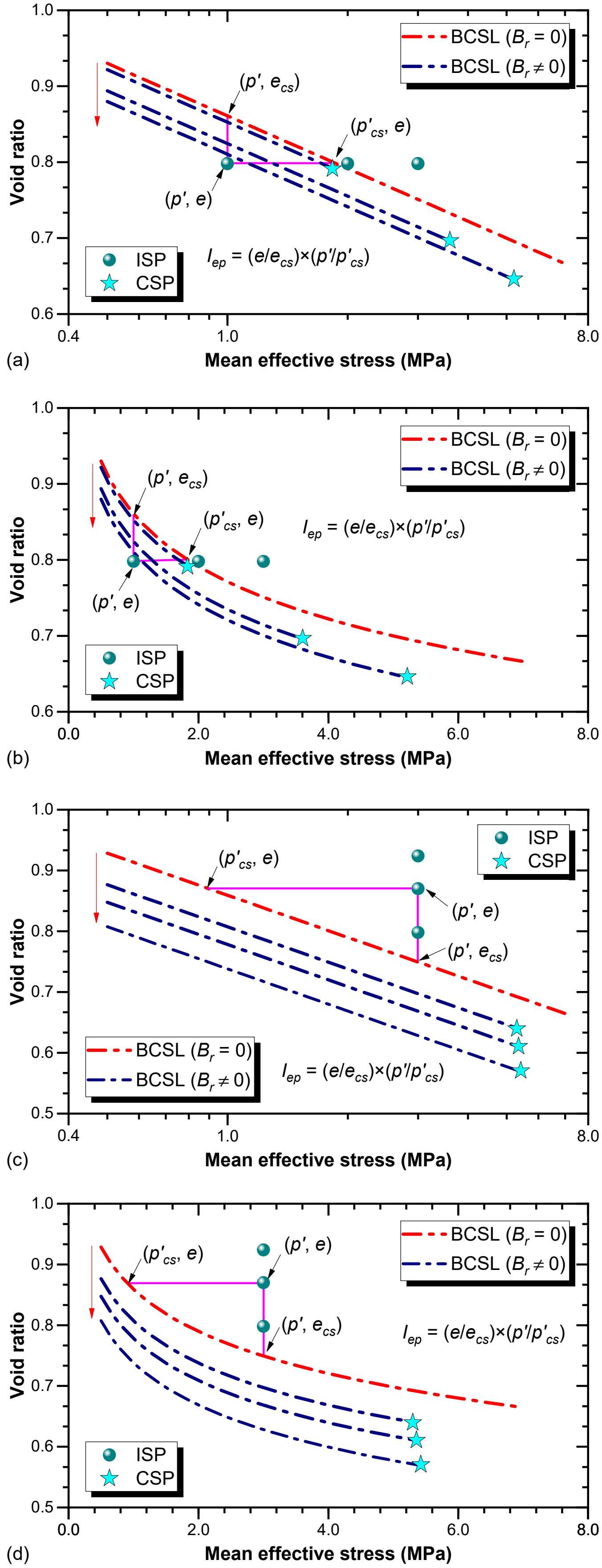

1.0
0.9
0.8
0.7
0.6
Void ratio
BCSL (B_r = 0)
BCSL (B_r ≠ 0)
(p', e_{cs})
(p'_{cs}, e)
(p', e)
ISP
CSP
I_{ep} = (e/e_{cs})×(p'/p'_{cs})
0.4
1.0
8.0
(a)
Mean effective stress (MPa)
0.0
2.0
4.0
6.0
8.0
(b)
0.5
(c)
(d)

Fig 2 size: Width = One column (i.e., 8.8 cm); DPI = 600

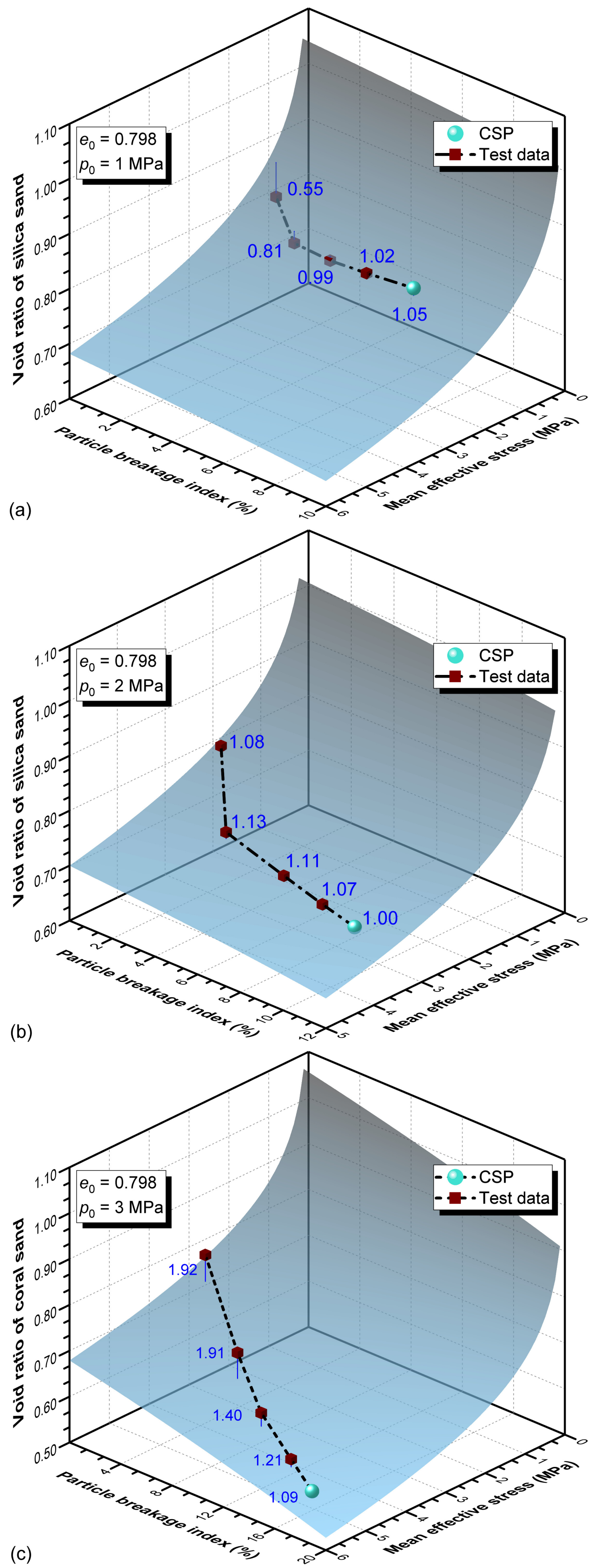

Fig 3 size: Width = One column (i.e., 8.8 cm); DPI = 600

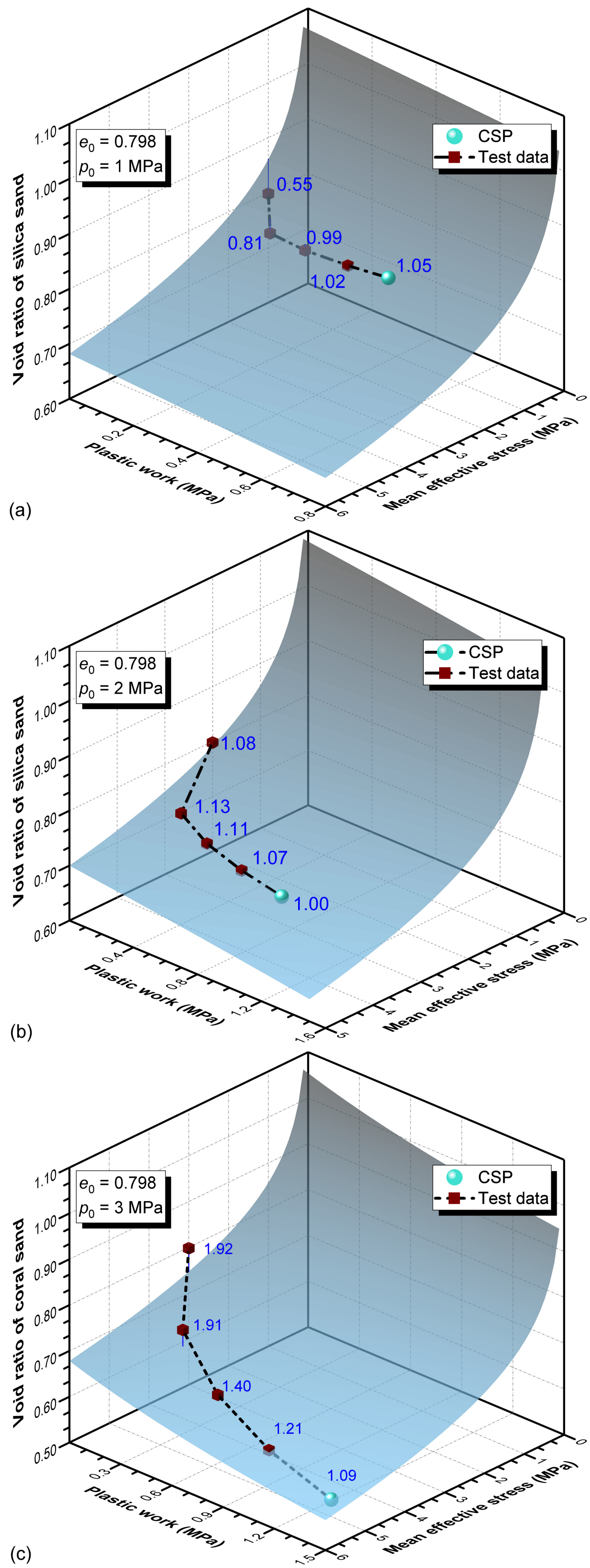

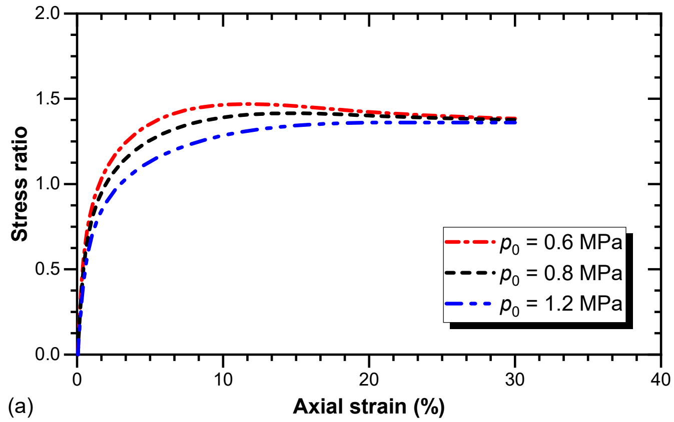
Stress ratio
Axial strain (%)
p0 = 0.6 MPa
p0 = 0.8 MPa
p0 = 1.2 MPa
0.0
0.5
1.0
1.5
2.0
0
10
20
30
40
(a)

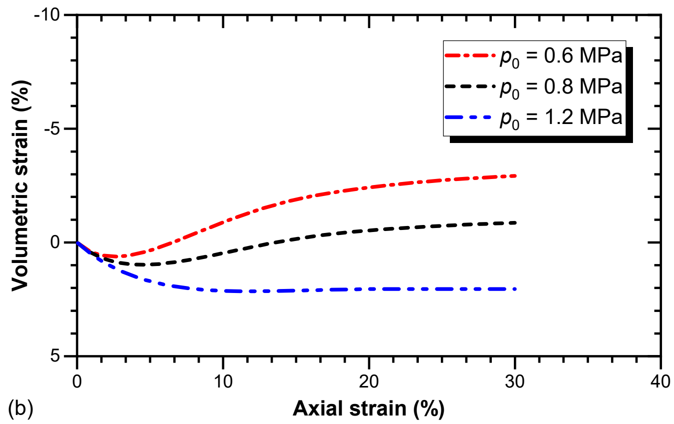
Volumetric strain (%)
Axial strain (%)
p0 = 0.6 MPa
p0 = 0.8 MPa
p0 = 1.2 MPa
-10
-5
0
5
(b)

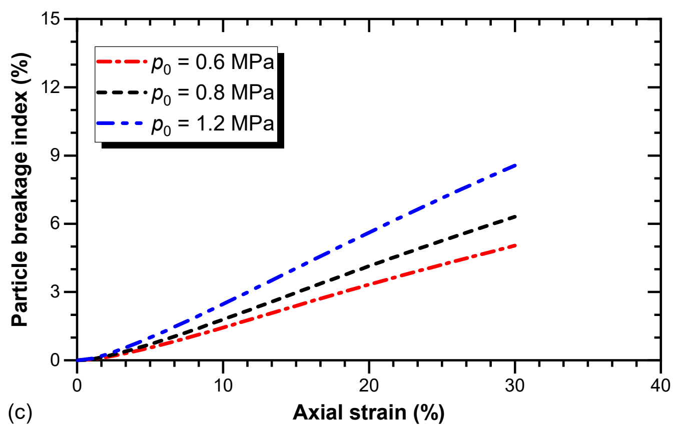
Particle breakage index (%)
Axial strain (%)
p0 = 0.6 MPa
p0 = 0.8 MPa
p0 = 1.2 MPa
0
3
6
9
12
15
(c)

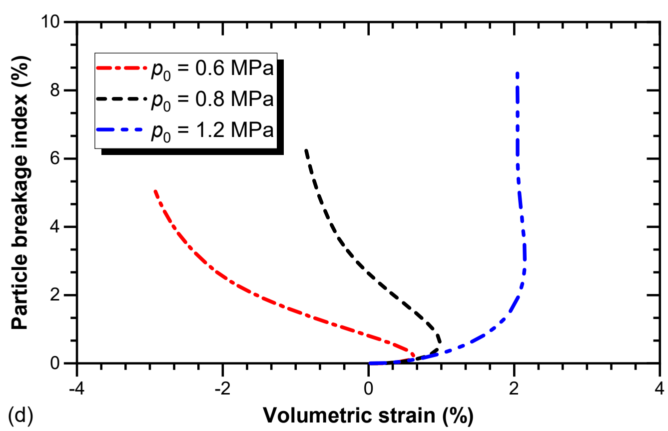
Particle breakage index (%)
Volumetric strain (%)
p0 = 0.6 MPa
p0 = 0.8 MPa
p0 = 1.2 MPa
0
2
4
6
8
10
-4
-2
0
2
4
(d)

Fig 5 size: Width = One column (i.e., 8.8 cm); DPI = 600

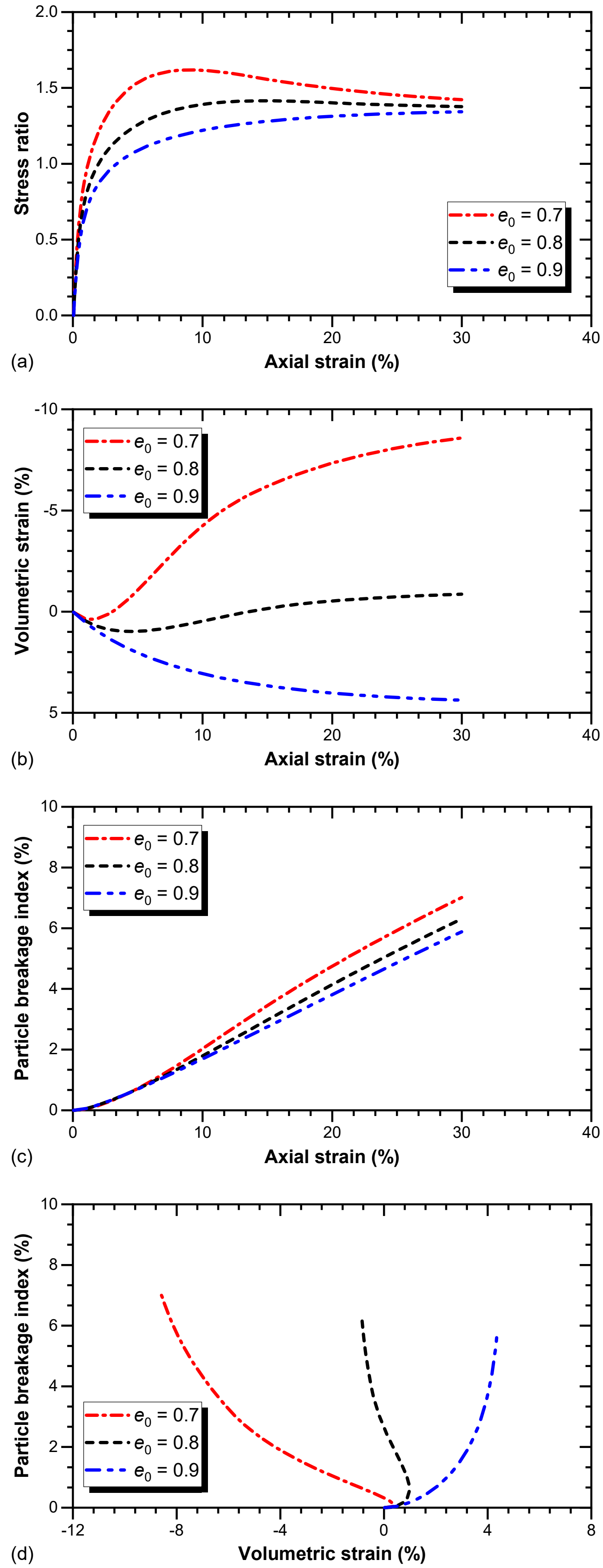

Fig 6 size: Width = One column (i.e., 8.8 cm); DPI = 600

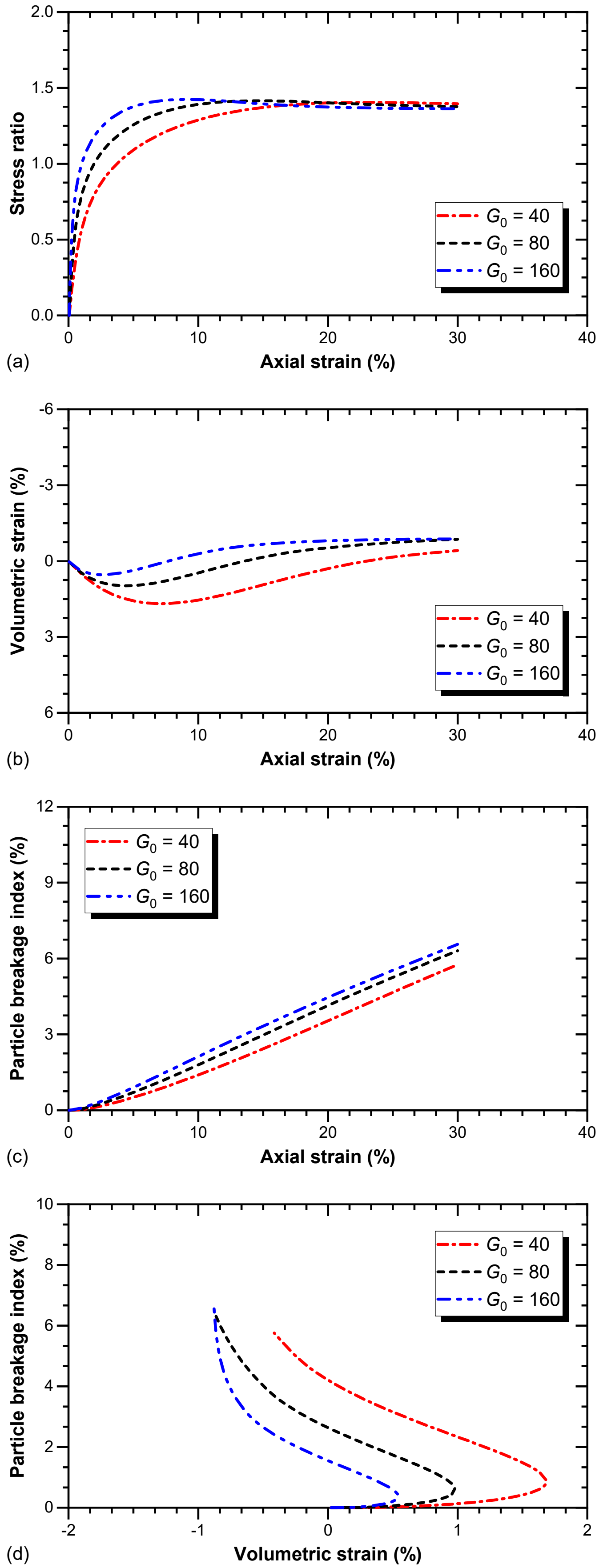

Fig 7 size: Width = One column (i.e., 8.8 cm); DPI = 600

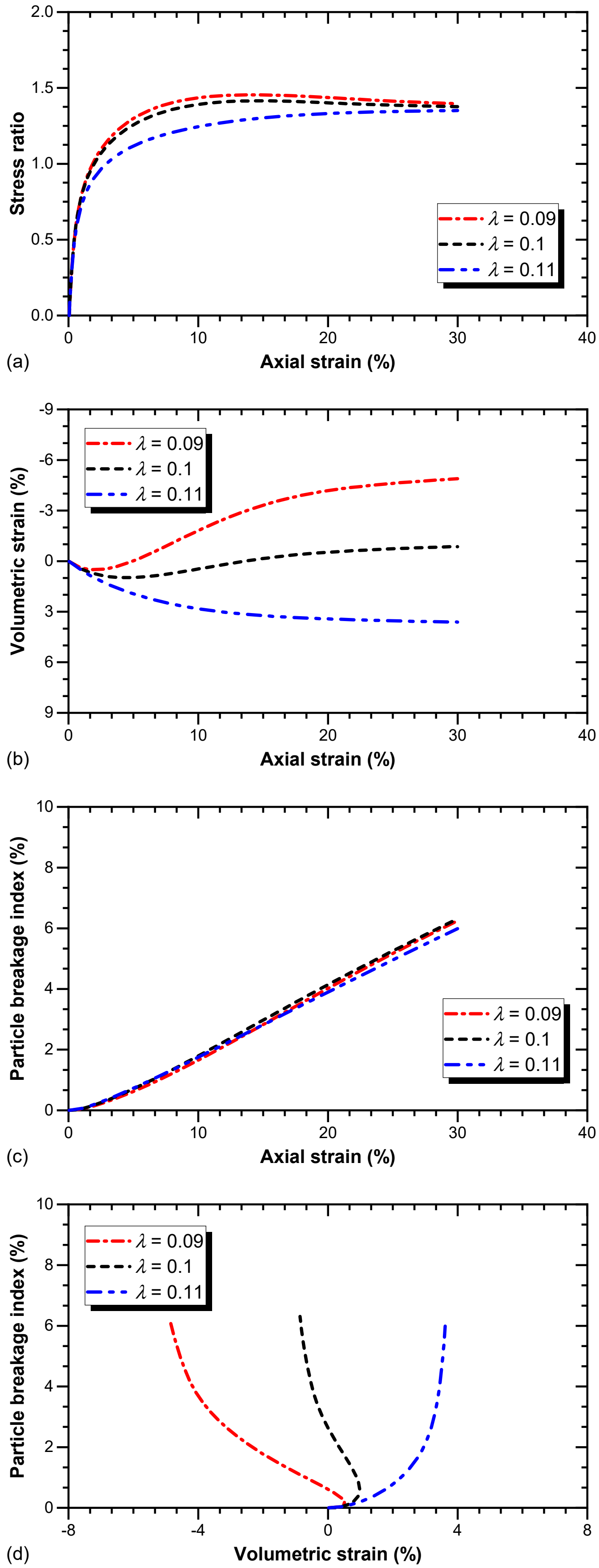

Fig 8 size: Width = One column (i.e., 8.8 cm); DPI = 600

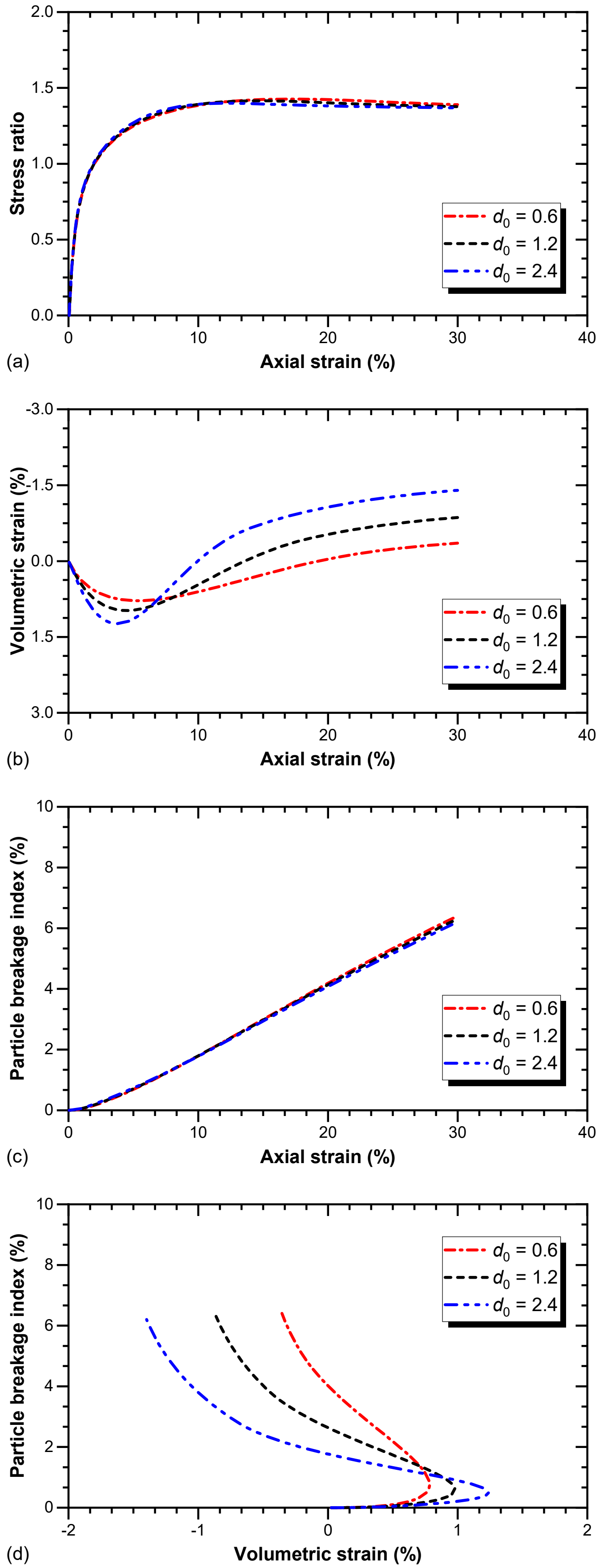

Fig 9 size: Width = One column (i.e., 8.8 cm); DPI = 600

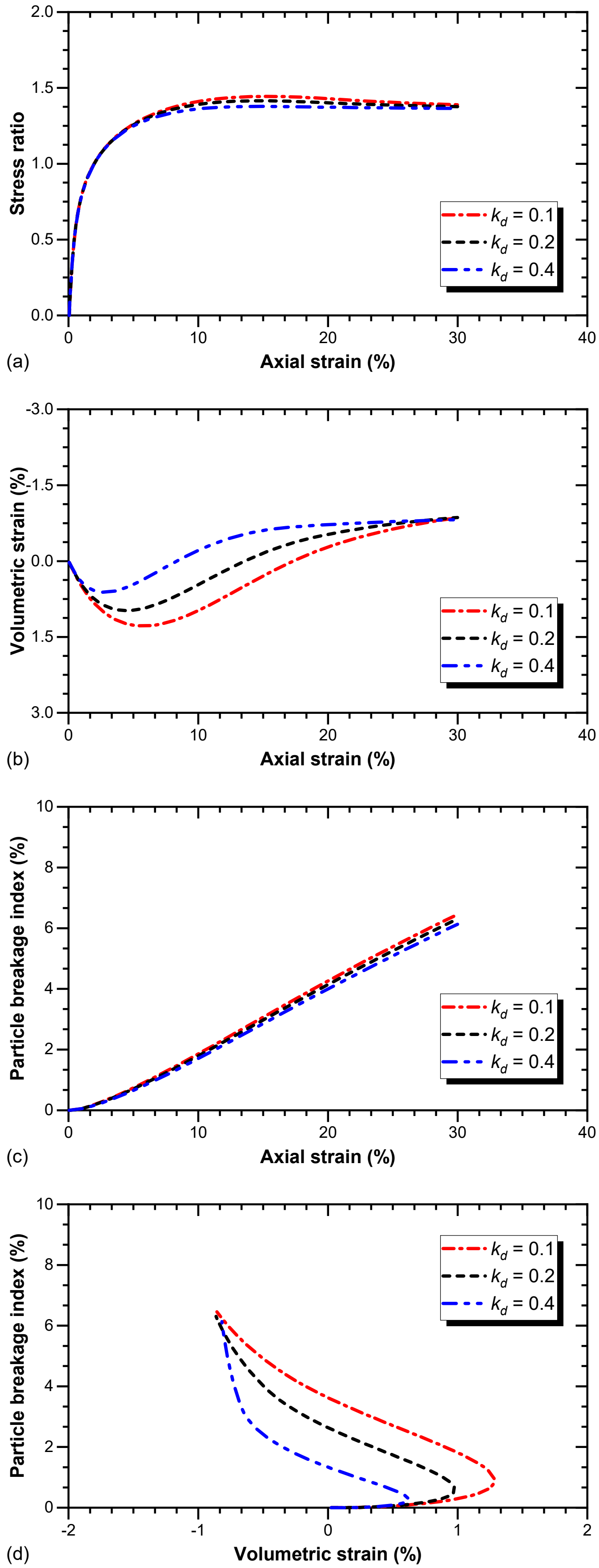

Fig 10 size: Width = One column (i.e., 8.8 cm); DPI = 600

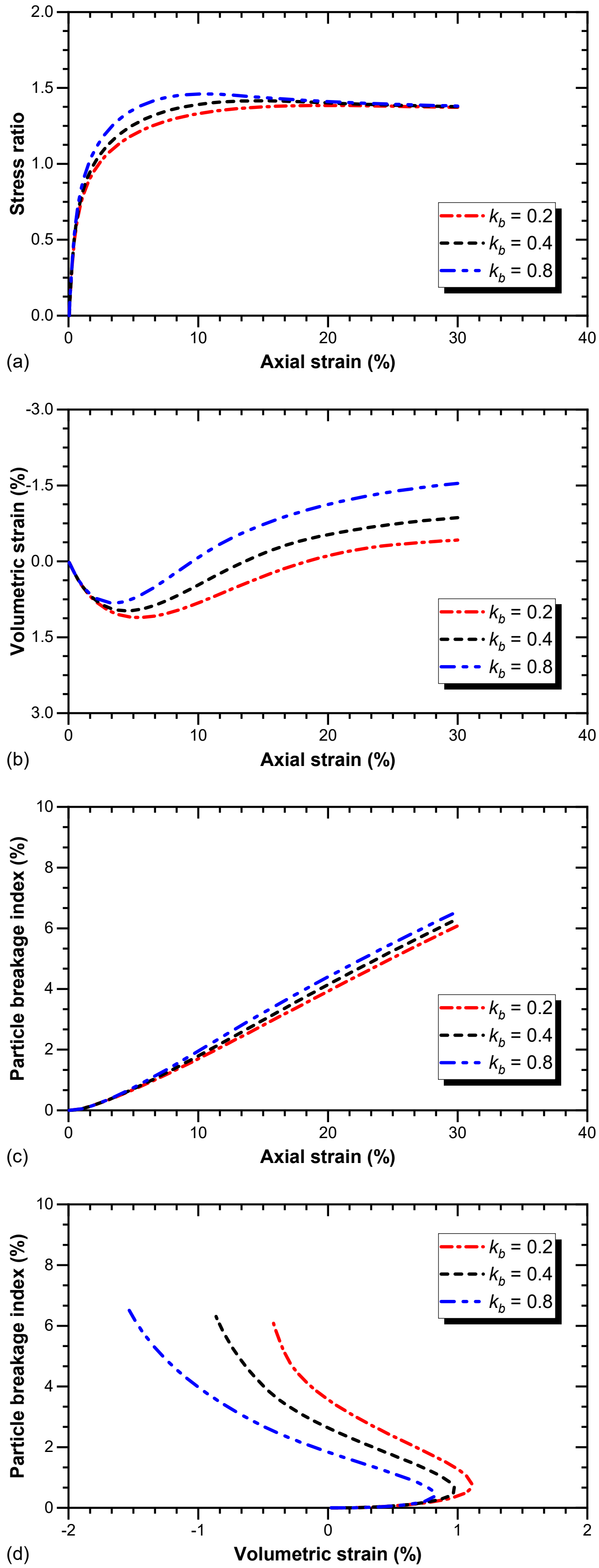

Fig 11 size: Width = One column (i.e., 8.8 cm); DPI = 600 Click here to access/download;Figure;Fig 11.pdf

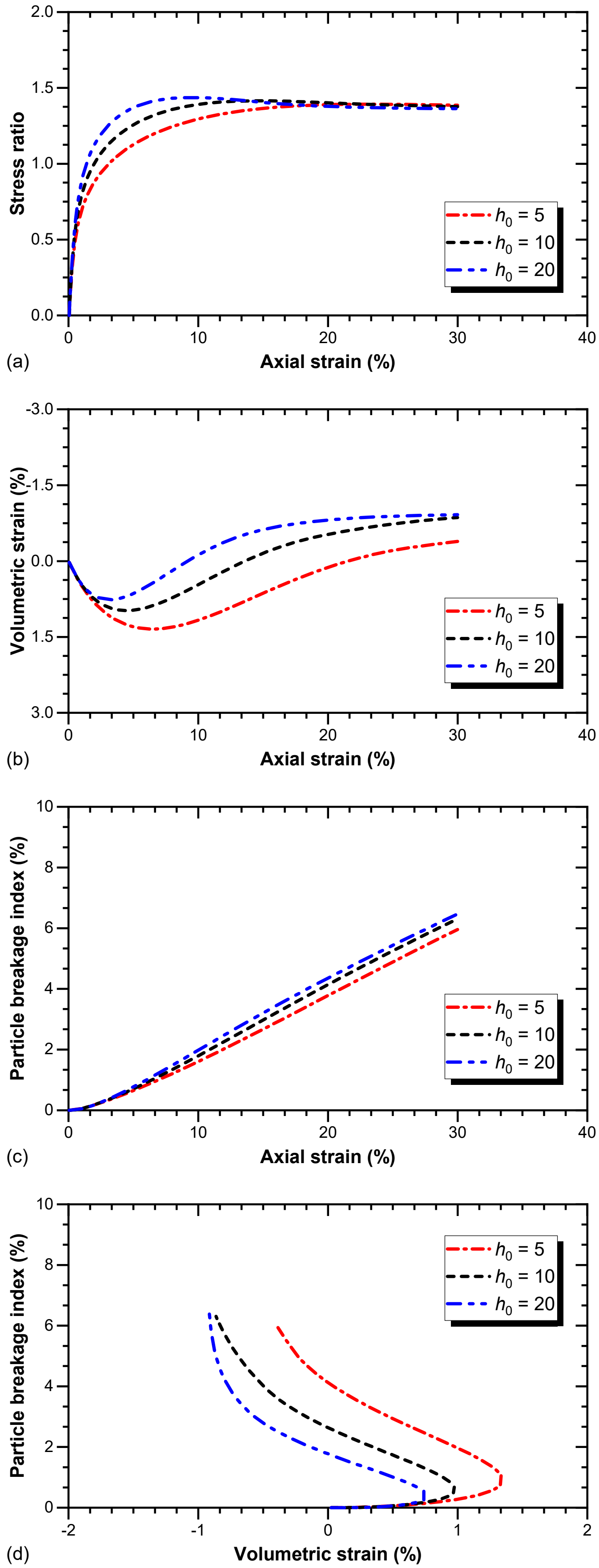

Fig 12 size: Width = One column (i.e., 8.8 cm); DPI = 600

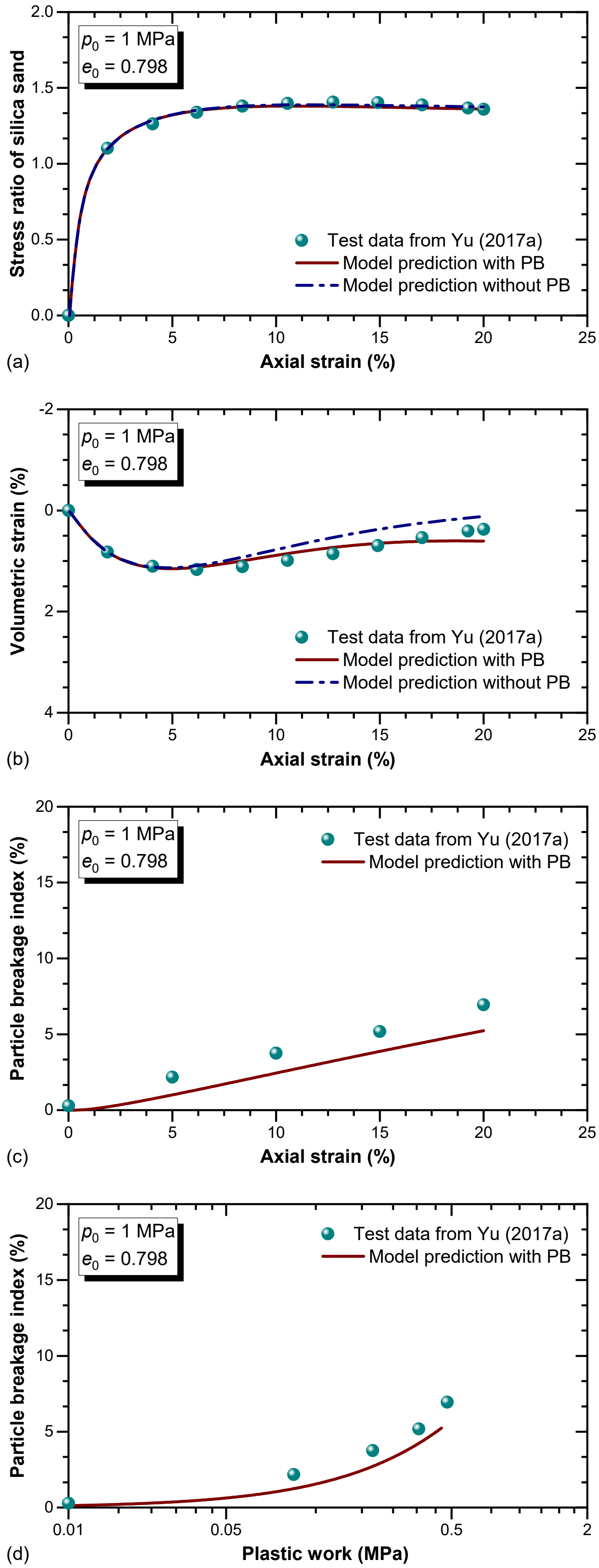

Fig 13 size: Width = One column (i.e., 8.8 cm); DPI = 600

Click here to access/download;Figure;Fig 13.pdf

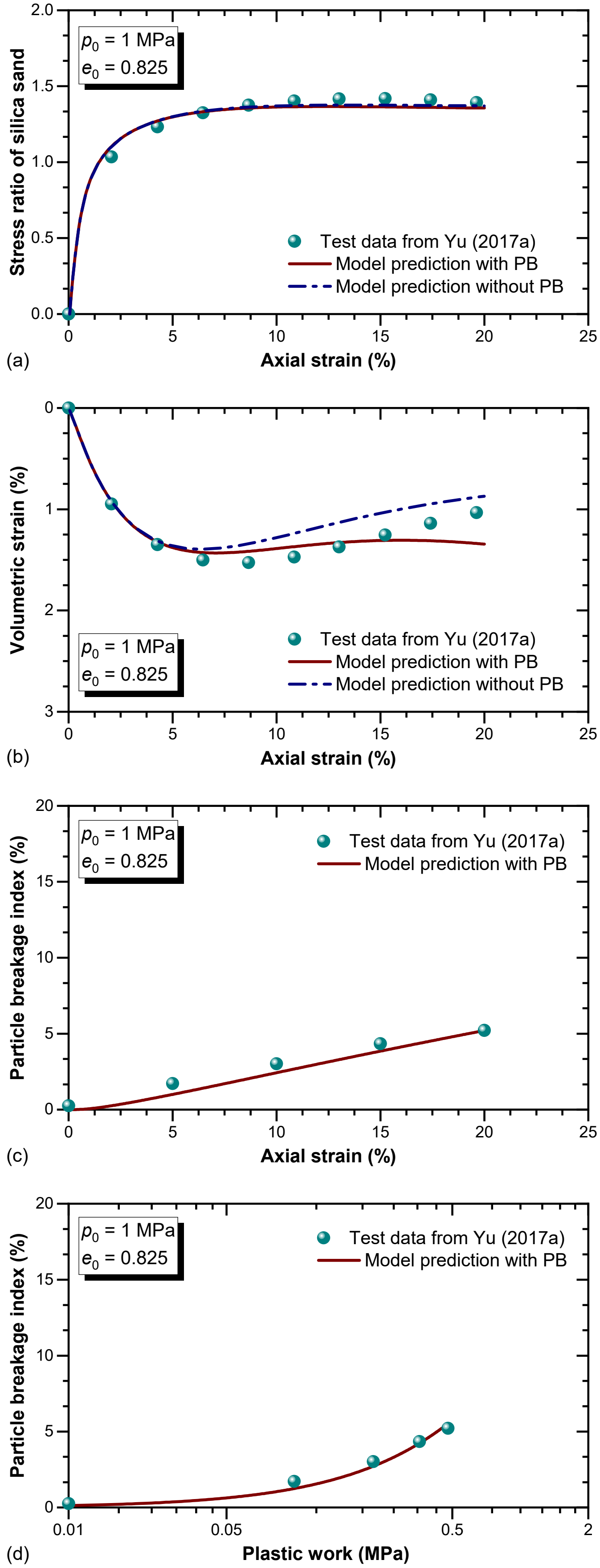

Fig 14 size: Width = One column (i.e., 8.8 cm); DPI = 600 Click here to access/download;Figure;Fig 14.pdf

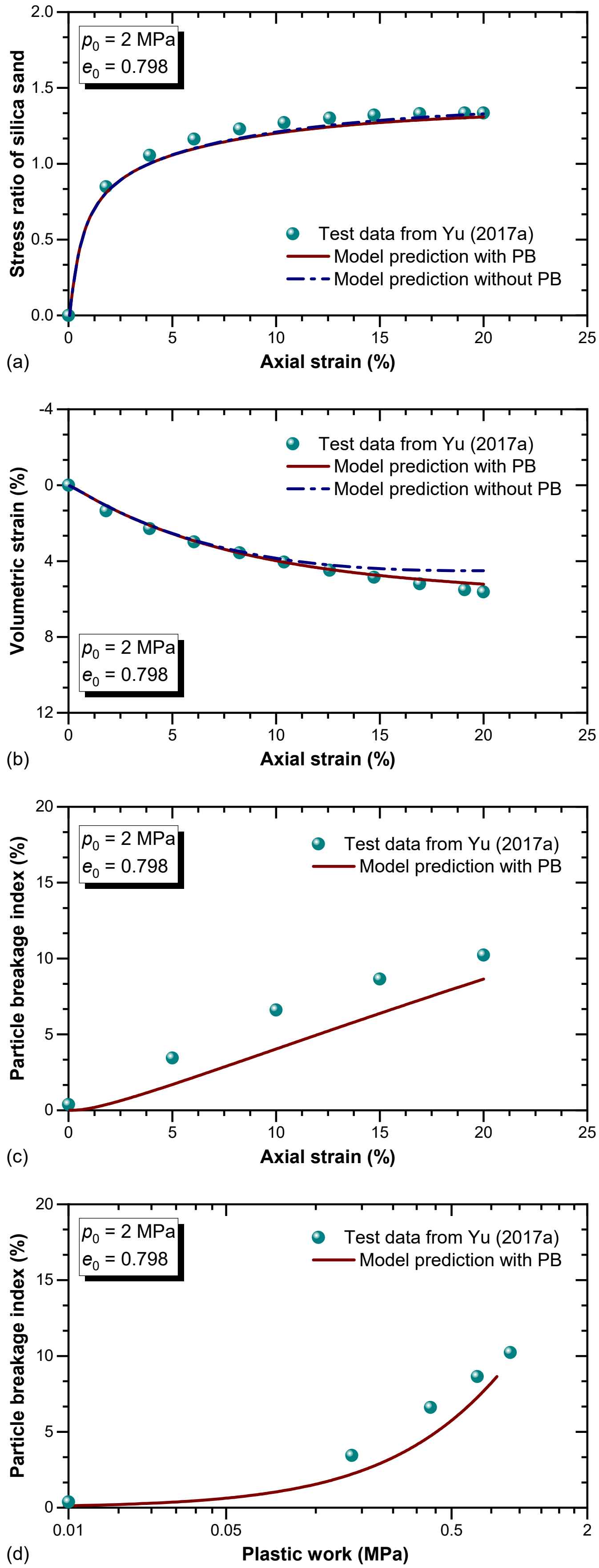

Fig 15 size: Width = One column (i.e., 8.8 cm); DPI = 600

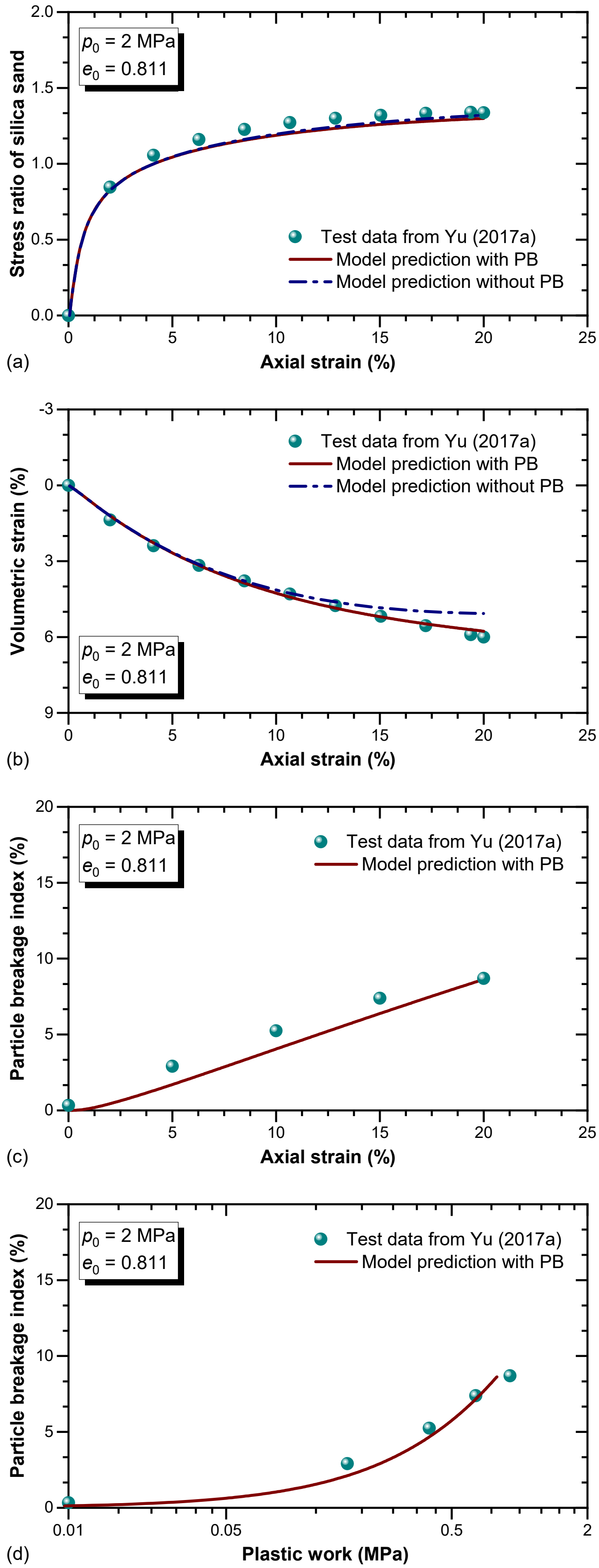

Fig 16 size: Width = One column (i.e., 8.8 cm); DPI = 600

Click here to access/download;Figure;Fig 16.pdf

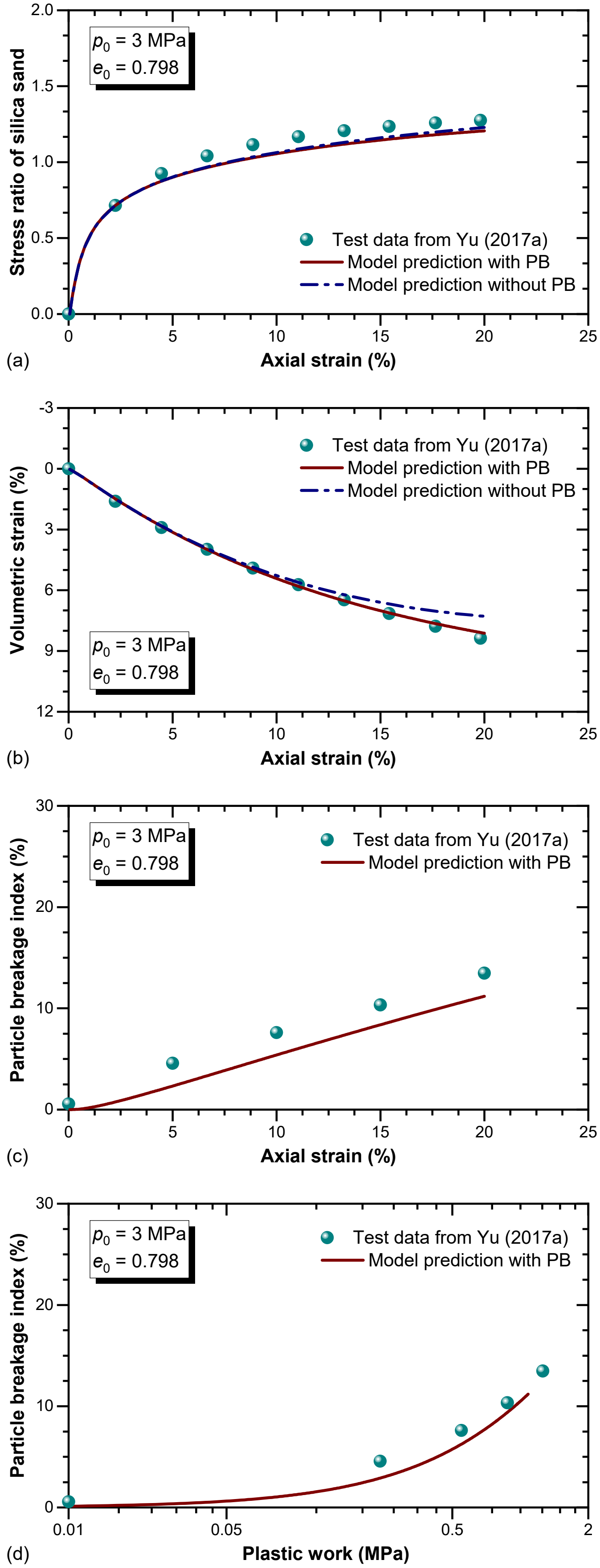

Fig 17 size: Width = One column (i.e., 8.8 cm); DPI = 600

Click here to access/download;Figure;Fig 17.pdf

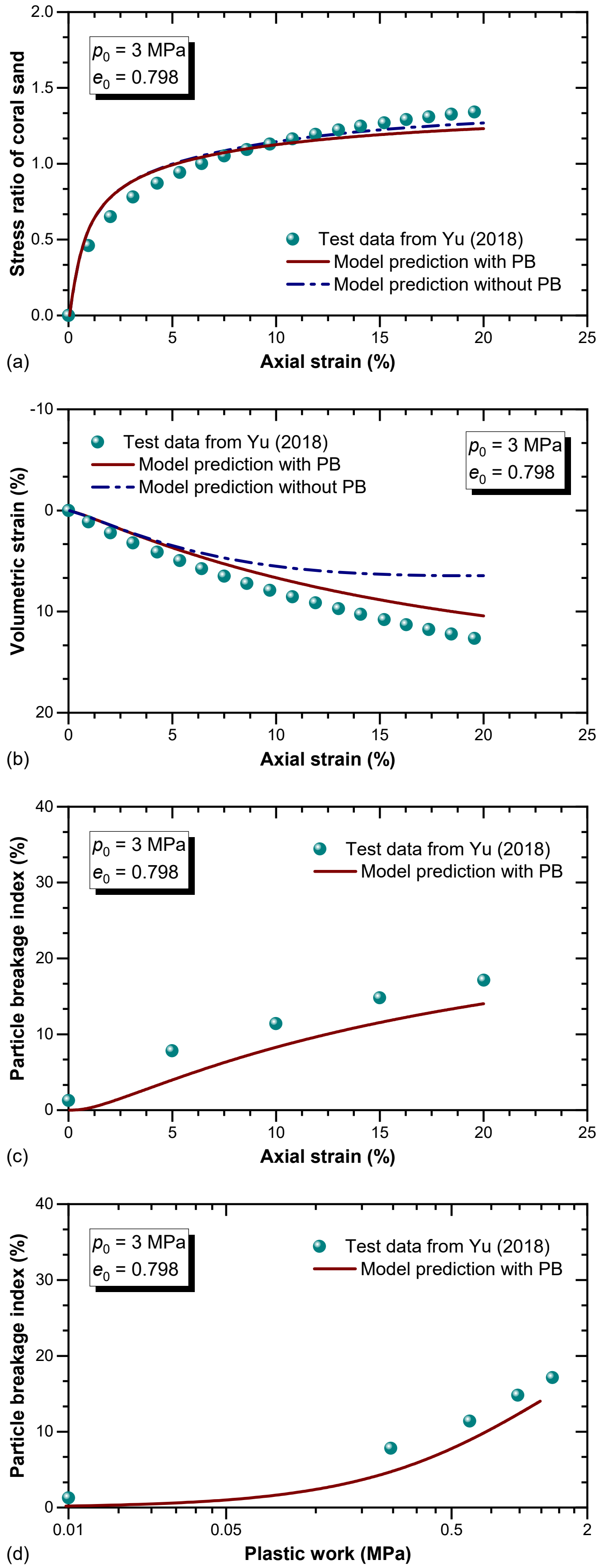

Fig 18 size: Width = One column (i.e., 8.8 cm); DPI = 600

Click here to access/download;Figure;Fig 18.pdf

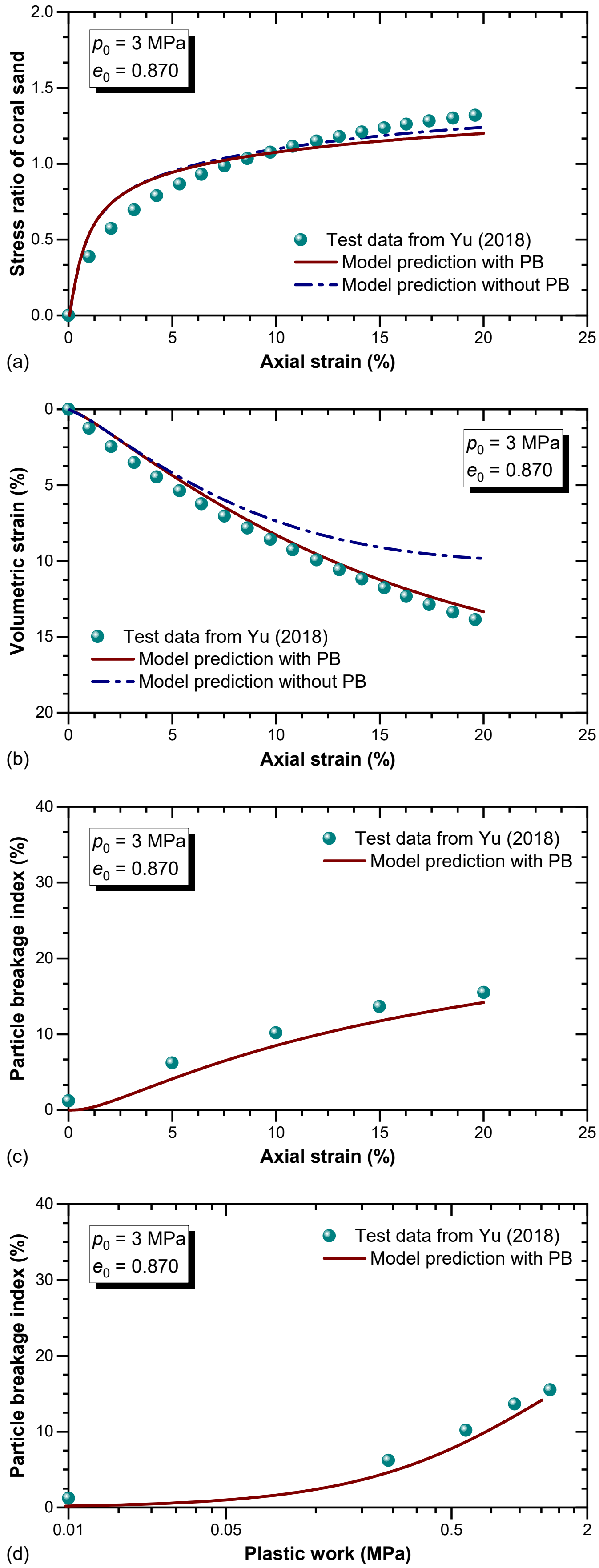

Fig 19 size: Width = One column (i.e., 8.8 cm); DPI = 600 Click here to access/download;Figure;Fig 19.pdf

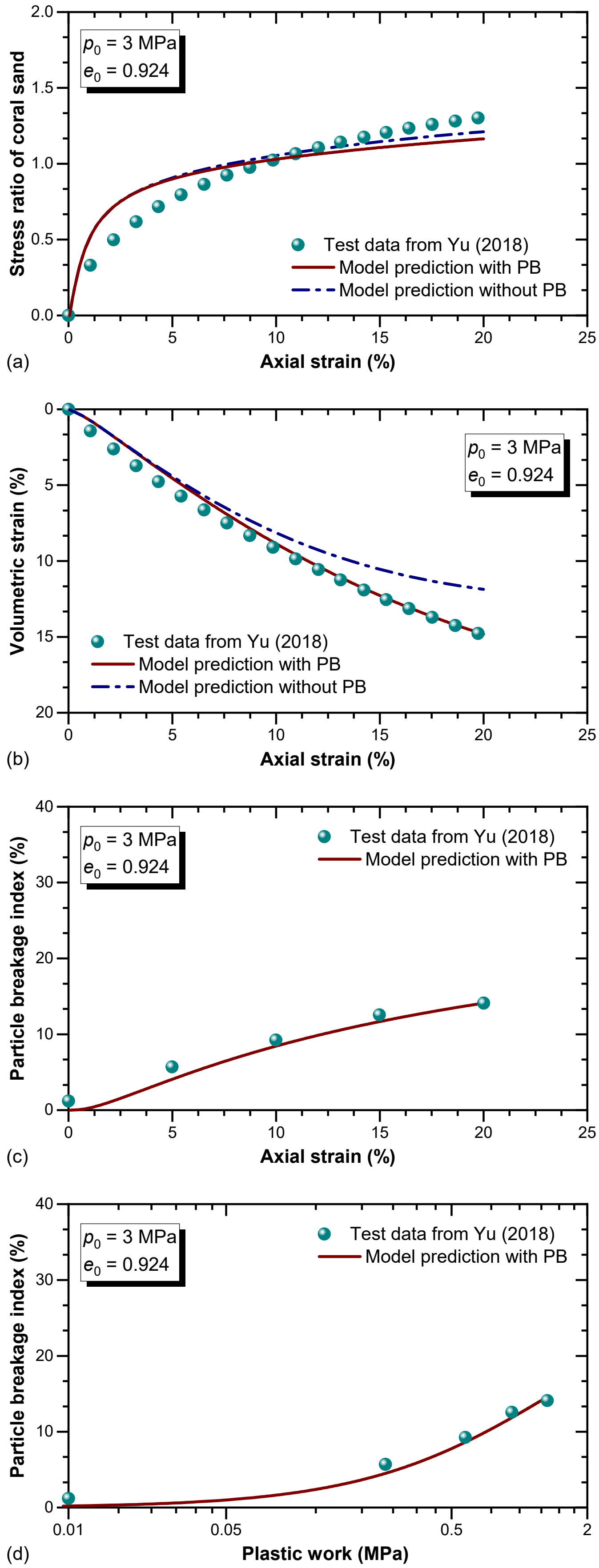

Fig 20 size: Width = One column (i.e., 8.8 cm); DPI = 600 Click here to access/download;Figure;Fig 20.pdf

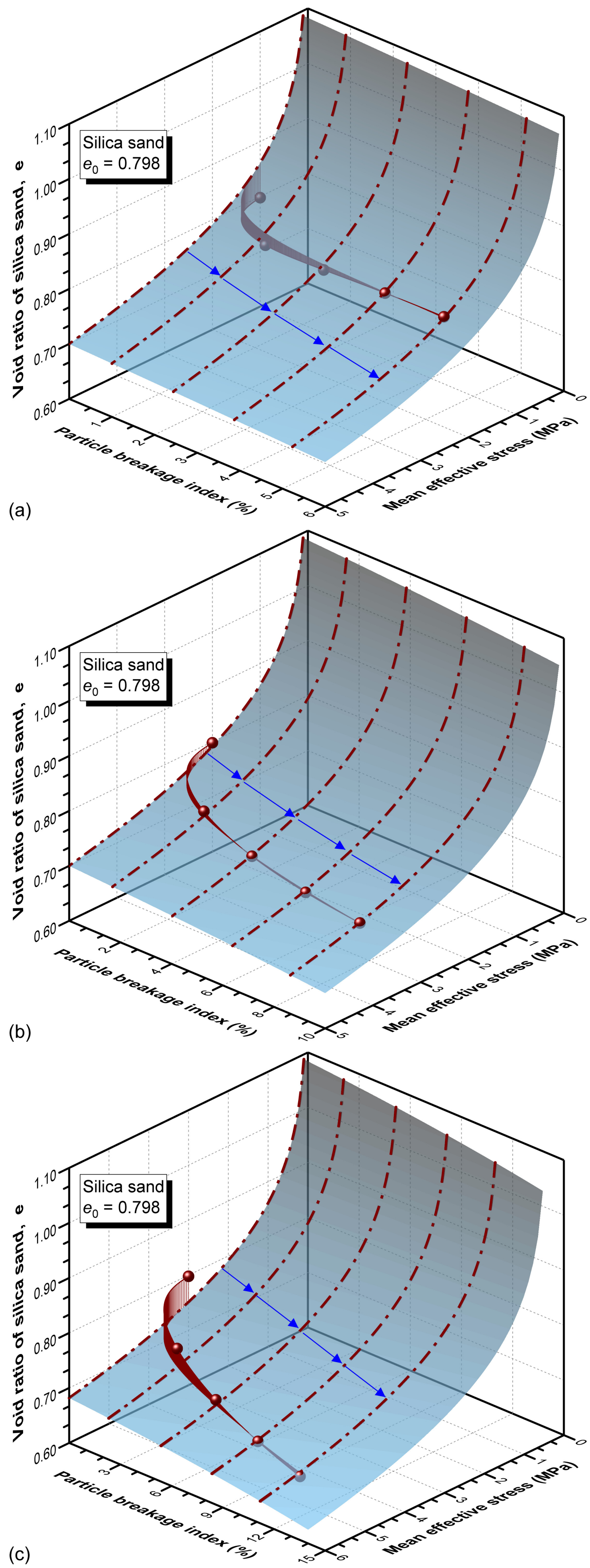

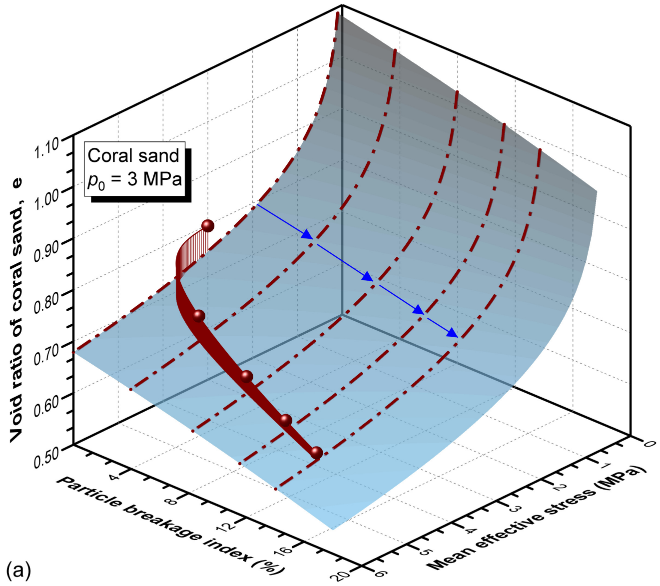
Coral sand
p_0 = 3 MPa
Void ratio of coral sand, e
Particle breakage index (%)
Mean effective stress (MPa)

(a)

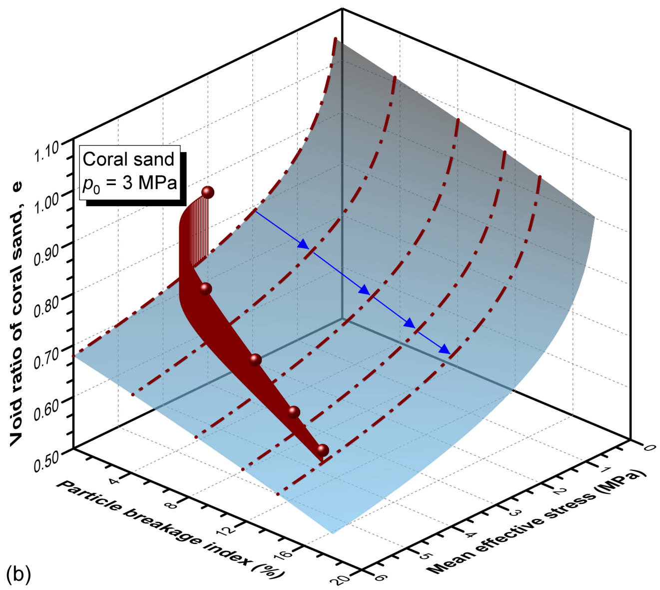
Coral sand
p_0 = 3 MPa
Void ratio of coral sand, e
Particle breakage index (%)
Mean effective stress (MPa)

(b)

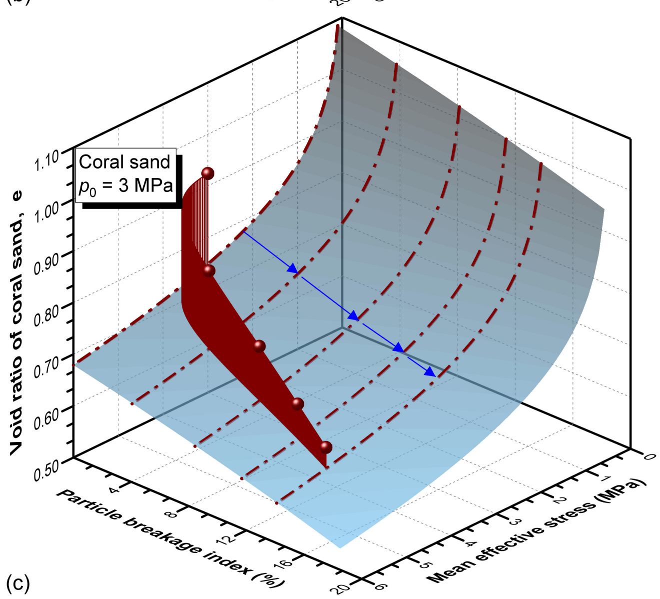
Coral sand
p_0 = 3 MPa
Void ratio of coral sand, e
Particle breakage index (%)
Mean effective stress (MPa)

(c)

Fig 22 size: Width = One column (i.e., 8.8 cm); DPI = 600

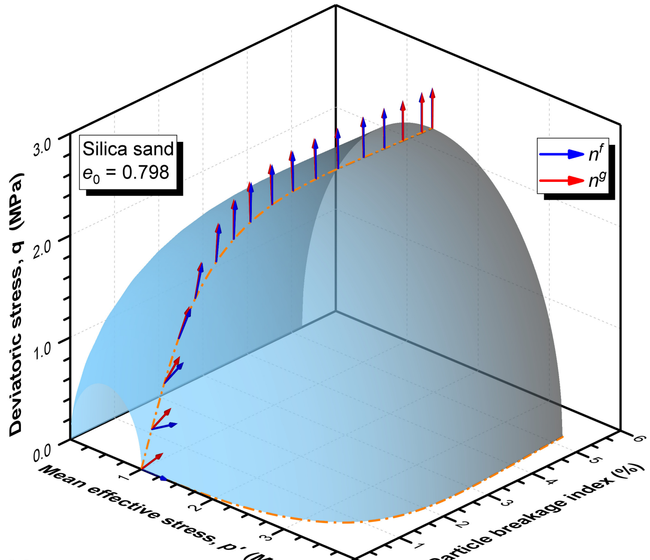

(a)

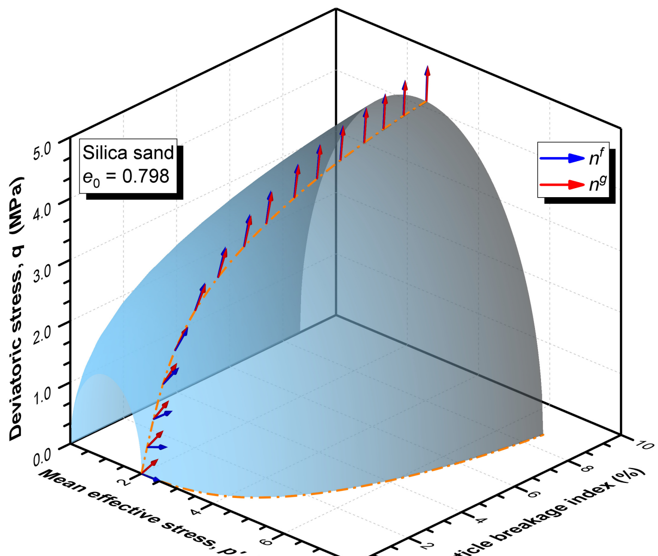

(b)

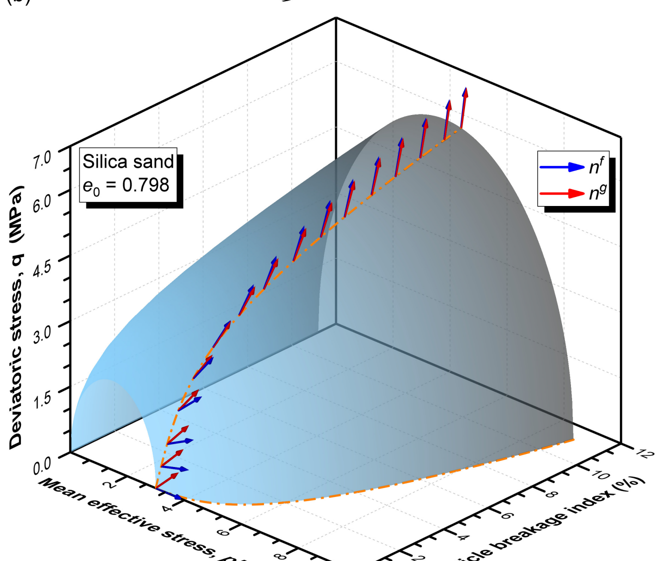

(c)

Fig 23 size: Width = One column (i.e., 8.8 cm); DPI = 600 Click here to access/download;Figure;Fig 23.pdf

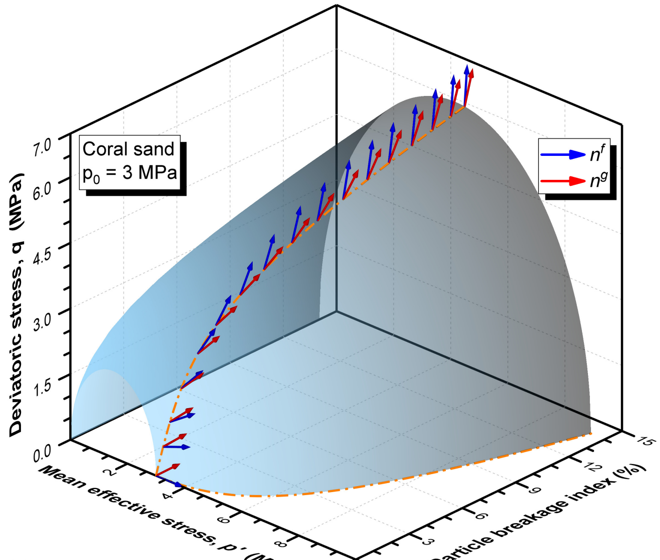

(a)

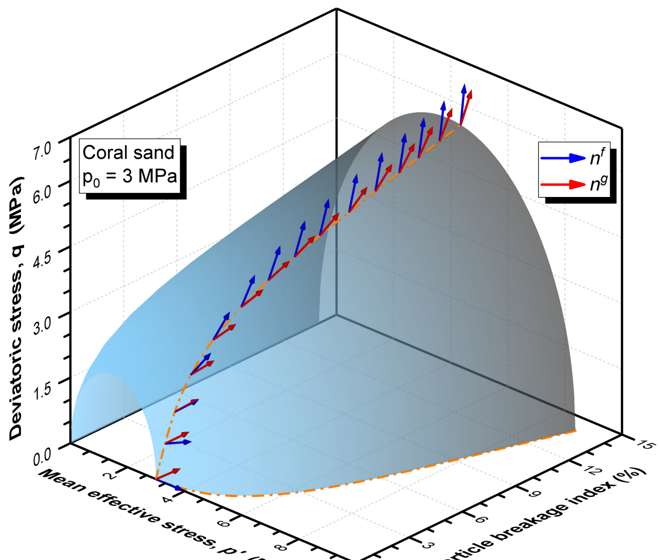

(b)

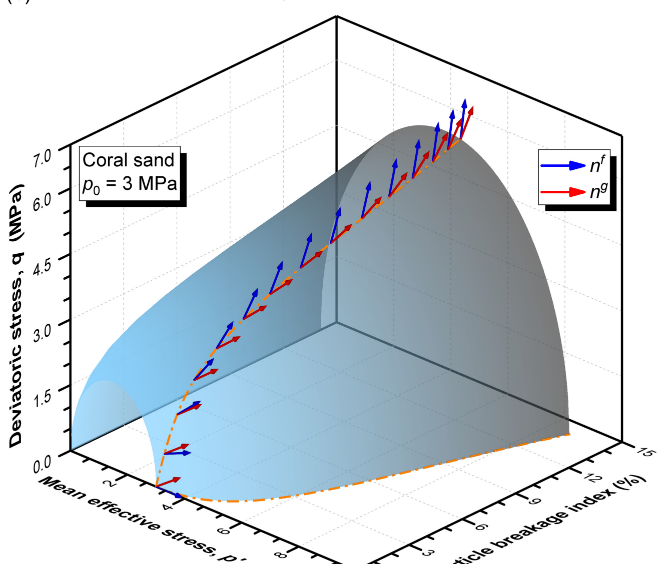

(c)